

DIPLOMARBEIT

An Experimental Study of Transition to Turbulence in Plane Poiseuille Flow

ausgeführt zum Zwecke der Erlangung des akademischen Grades eines

Diplom-Ingenieurs

unter der Leitung von

Univ.Prof. Dipl.-Phys. Dr. rer. nat. habil. Hendrik KUHLMANN
Institut für Strömungsmechanik und Wärmeübertragung (E322)

eingereicht an der

Technischen Universität Wien

Fakultät für Maschinenwesen und Betriebswissenschaften

von

Michael Philip SITTE, MPhil

Matr.Nr. 0826322

Freyung 6/4/9, 1010 Wien

Wien am 21. August 2014

Michael Philip Sitte

Acknowledgements

This work was supervised by Univ.Prof. Dr. Hendrik Kuhlmann, *Institut für Strömungsmechanik und Wärmeübertragung* at *Vienna University of Technology*. The experimental work was carried out at *Institute of Science and Technology Austria (IST Austria)* with the support kindly provided by Univ.Prof. Dr. Björn Hof.

At first, I would like to thank my supervisor Univ.Prof. Dr. Hendrik Kuhlmann for offering me the opportunity to participate in this project. My gratitude also goes to Dr. Jakob Kühnen for arranging this cooperation. Furthermore, I am very grateful to Univ.Prof. Dr. Björn Hof and the members of his group for the great time I have spent working at *IST Austria*. It was both a very pleasant and instructive experience.

Most of all, I would like to thank Dr. Mukund Vasudevan for the continuous support he has provided me with during this project. Mukund, it has been a pleasure and privilege to worked with you. Thank you so much for your invaluable advice and the great feedback you have given me. I am also thankful for many great discussions we have had and, last but not least, I have much appreciated that you introduced me to some delicious Indian curry during lunch time at *IST*.

Zusammenfassung

Der laminar-turbulente Umschlag einer druckgetriebenen Strömung zwischen zwei parallelen Platten, auch ebene Poiseuille Strömung genannt, wird mit Hilfe einer Methode zur Strömungsvisualisierung untersucht. Dieser Übergangsprozess ist subkritisch, sodass währenddessen laminare und turbulente Bereiche in der Strömung gleichzeitig vorhanden sind. Der Fokus dieser Arbeit liegt auf der zeitlichen Entwicklung dieser räumlich beschränkten, turbulenten Bereiche in einem experimentellen Kanal großer Breite und Länge.

Zu diesem Zweck werden ovale Wirbelflecken unter Zuhilfenahme von lokalen Störungen einzeln ausgelöst und deren zeitliche Entwicklung verfolgt, wobei auffällt dass diese Flecken eine Streifenform ausbilden. Deshalb wurde ein neuer Störmechanismus entworfen, mit dem die Entstehung solcher Streifen in der Strömung direkt angeregt werden können. Hierdurch konnte gezeigt werden, dass, erstens, diese Streifen die natürlich vorkommende Form lokal beschränkter Turbulenz darstellen und, zweitens, dass diese Streifen in einem deutlich niedrigeren Bereich von Reynolds-Zahlen bestehen können, als bisher geglaubt.

Es konnte auch gezeigt werden, dass diese Streifen einen ausgezeichneten Winkel relativ zur Fließrichtung annehmen. Diese Winkel liegen in einem engen Bereich dessen Grenzen von der Reynolds-Zahl abhängen. Außerdem werden Zu- und Abnahme der Größe von existierenden Streifen, sowie die Keimbildung neuer Bänder detailliert beschrieben. Zum Schluss wurde der kritische Punkt für den turbulenten Umschlag einer ebenen Poiseuilleströmung aus den durchschnittlichen Zuwachs- bzw. Abklingraten abgeleitet. Dieser Schwellwert, unter welchem alle turbulenten Strukturen abklingen, liegt deutlich tiefer als alle bisherigen Schätzungen.

Abstract

The laminar-turbulent transition of a pressure driven flow between two parallel plates, called plane Poiseuille flow, is studied using a flow visualisation technique. The transition process in the sub-critical regime is characterised by the co-existence of laminar and turbulent regions. The present work focuses on the evolution of localised turbulence in a channel with a large aspect ratio and length.

For this purpose, individual spot-shaped structures are triggered via a localised perturbation. Their development is monitored in time, which shows that these turbulent spots grow into the shape of stripes. Consequently, a new perturbation technique is developed that directly excites localised stripes in the flow. It is shown that the stripes are the natural form of localised turbulence and that they can exist at Reynolds numbers much lower than previously believed.

It is also shown that these stripes are inclined to the mean flow direction in a narrow range of angles which depends on the Reynolds number. Furthermore, the growth and decay of existing turbulent stripes and the nucleation of new stripes is described in detail. Finally, the average growth and decay rates of these stripes are used to deduce the critical point in plane Poiseuille flow, below which turbulence cannot be sustained. This critical number is lower than existing estimates in the literature.

Contents

Contents	v
List of Figures	vi
Nomenclature	vii
1 Introduction	1
1.1 Motivation	1
1.2 Objectives	3
1.3 Background	3
1.4 Outline	8
2 Methodology	10
2.1 Experimental Set-Up	10
2.2 Perturbation method	12
2.2.1 Localised Perturbation	13
2.2.2 Extended Perturbation	14
2.2.3 Disturbed Inlet Flow	15
2.3 Flow Visualisation	17
2.4 Image Processing	19
2.5 Error Estimates	20
3 Results and Discussion	22
3.1 Properties of the Channel Flow	22
3.1.1 Transition to Turbulence	22
3.1.2 Pressure Drop	22

CONTENTS

3.2	Characteristics of Turbulent Spots	24
3.2.1	Typical Development of a Turbulent Spot	24
3.2.2	Spreading of the Turbulent Spot	27
3.3	Growth and Decay Rates	30
3.4	Characteristics of Turbulent Stripes	33
3.4.1	Typical Development of Turbulent Stripes	35
3.4.2	Branching of Turbulent Stripes	37
3.4.3	Natural Angle of Turbulent Stripes	39
3.5	Critical Point in Plane Poiseuille Flow	43
4	Conclusion	47
4.1	Summary of the Results	47
4.2	Outlook	49
	Bibliography	50
	Curriculum Vitae	54

List of Figures

1.1	Schematic of a plane Poiseuille flow.	5
2.1	Experimental set-up.	12
2.2	Injected volume as a function of supply pressure.	14
2.3	Triggering mechanism.	16
2.4	Velocity of the extend perturbation mechanism vs. time.	16
3.1	Friction factor f	24
3.2	Development of a turbulent spot at $Re_m = 1300$	28
3.3	A turbulent spot at $Re_m = 1500$	29
3.4	Schematic for the spreading angle of a turbulent spot.	30
3.5	Variation of the spreading angle with the Reynolds number.	30
3.6	Position of the spot's leading and trailing edge in time.	31
3.7	Evolution of the average area of a turbulent spot.	33
3.8	Size distribution of turbulent spots at various positions.	34
3.9	Probability of decay for a turbulent spot.	34
3.10	Development of a turbulent stripe at $Re_m = 1100$	38
3.11	Image sequence of a splitting event at $Re_m = 1200$	40
3.12	The evolution of the angle of a turbulent stripe.	44
3.13	Growth and decay of a turbulent stripe as a function of the trigger-angle.	44
3.14	The natural angle as a function of Reynolds number.	44
3.15	PDFs for the distribution for the angle of turbulent stripes.	45
3.16	Growth of turbulent stripes as a function of Reynolds number.	46

Nomenclature

Roman letters

A	Area of a spot or stipe
f	Darcy friction factor
h	Channel height
L_x	Channel length
L_z	Channel width
p	Pressure
Q	Flow rate
Re_c	Unconditional stability thresholds
Re_g	Global stability thresholds, <i>critical</i> Reynolds number
Re_m	Reynolds number based on channel height ($= U_b h/\nu$)
t	Time
t^*	Dimensionless time in advective units ($= tU_b/h$)
U_b	Bulk velocity
W	Span-wise extent of the stripe
x	Coordinate along the length of the channel
x^*	Non-dimensional stream-wise coordinate ($= x/h$)
z	Coordinate along the width of the channel
z^*	Non-dimensional span-wise coordinate ($= z/h$)

Greek letters

α	Inclination of the stripe to the stream-wise direction
α_0	Initial angle of the stripe
α_n	Natural angle of a stripe

α_{trig}	Trigger angle
μ	Dynamic viscosity
ν	Kinematic viscosity
ϕ	Volume fraction
ρ	Density

Other symbols

2D	Two dimensional
3D	Three dimensional
DNS	Direct numerical simulation
HPF	Hagen Poiseuille flow (pipe flow)
PDF	Probability density function
PCF	Plane Couette flow
PPF	Plane Poiseuille flow (channel flow)
TCF	Taylor Couette flow

Chapter 1

Introduction

1.1 Motivation

Turbulent transition denotes the transition process from a well-ordered laminar to a turbulent flow. Turbulence is generally characterised by unsteadiness, three-dimensionality and chaotic fluid motion. It is thus dissipative and increases the mechanical drag as well as mixing compared to a laminar flow, which makes it relevant in a multitude of engineering applications. Studying the onset of turbulence relates to the understanding of the mechanisms involved in this transition process. Ultimately this is motivated by the objective of controlling the onset of turbulence.

In the case of various flows, the process of turbulent transition is supercritical. These flows are linearly unstable such that infinitesimal perturbations grow exponentially. Two examples are Rayleigh-Bénard cells or Taylor vortices. In phase space, the system increases the distance from the base state continuously while it moves towards an unstable mode. The supercritical scenario to transition follows a series of bifurcations where successive states are always close to each other. Hence, linear stability theory and the classic tools from weakly non-linear analysis can be applied. Eventually, this transition process leads to turbulence [1, 2].

In contrast, the transition scenario of many wall-bound shear flows is subcritical. This means that transition to turbulence takes place although the flow

is linearly stable. Hence, a finite size perturbation is needed to start the transition process [3]. This scenario is much less understood since it can only be approached by determining stable solutions that, in the phase space are located at a finite distance from the base state [1].

An important characteristic of these subcritical systems is that different locally stable states co-exist in phase space. The consequence of this in the physical space is the development of homogeneous regions of both states, laminar and turbulent, that are in competition with each other and that are separated by clear fronts [4]. Hence, it has been suggested that the spatio-temporally intermittent character of turbulent transition in wall-bound shear flows could be explained as the nucleation problem related to a first-order phase transition. In particular, since the turbulent state is inherently chaotic, it was argued that it follows a stochastic contamination process such as that known for directed percolation [5].

In the case of a plane flow, the spatio-temporally intermittent character of the transition process manifests in the form of stripe patterns. In general, there have been several recent studies on small systems. They mainly focused on the temporal dynamics and some important findings have been made [6] (e.g. the *edge state* [7] or *localised solutions* [8]). Indeed, a spatially extremely limited system is sufficient to capture the local dynamics including the mechanisms that lead to turbulence. However, only extended domains, at least two orders of magnitude larger than the characteristic length of the flow, allow to study the development of turbulent-laminar patterns. In particular, the formation of these spatio-temporally intermittent structures is crucial to determine the transition threshold below which turbulence always decays [8]. According to Manneville [9], the use of very wide domains allows “...to approach the *thermodynamic limit* in the sense of statistical physics.”

One classical example of a subcritical transition is the pressure driven flow between to stationary, parallel plates, called plane Poiseuille flow (PPF). Yet, there are a very limited number of experimental studies. In particular, there is no recent work on the development of the intermittent patterns in extended domains. Hence, there is a need for an experimental study that can resolve the largest scales of intermittent patterns.

1.2 Objectives

In this thesis, turbulent transition in plane Poiseuille flow (PPF) is investigated experimentally. A channel of large aspect ratio and length is used and following a statistical approach the transitional range of Reynolds numbers is explored. The focus is on the development of *turbulent spots* and *stripes*, i.e. the coherent flow structures occurring in the spatio-temporally intermittent flow. In particular, it shall be shown that turbulent stripes can be produced and maintained at lower Reynolds numbers than previously suggested. For this purpose an novel perturbation technique is proposed that allows the production of extended disturbances. This new mechanism is used in addition to the localised perturbation employed by a large number of authors. Ultimately, the sum of observations and measurements shall be used to estimate a critical point for the existence of turbulence in PPF.

Through out the entire work, only the definition of the mean Reynolds number for PPF is used. It is given by $Re_m := U_b h / \nu$, where U_b is the bulk velocity, h the full channel height and ν the kinematic viscosity. The results from authors who use different characteristic scales to define the Reynolds number, are converted to Re_m , as defined here.

1.3 Background

The general context of this work is the transition from a laminar base flow to turbulence. The first scientific study on this phenomenon was conducted by Osborne Reynolds in 1883 [10]. He identified a single control parameter which is now known as the Reynolds number $Re = UL/\nu$, where U and L are characteristic velocity and length scales and ν the kinematic viscosity.

Manneville [11] reviews the general conditions of stability as a function of this parameter: Re_g is the *global stability* threshold below which whatever perturbation eventually decays and Re_c is the *unconditional* threshold above which infinitesimal perturbations grow. Hence Re_c can be calculated from linear stability analysis. For $Re_g < Re < Re_c$ the stability depends on the type and amplitude of the perturbation. In this range, the initial perturbation must

have a finite size in order to trigger a transition to turbulence. Furthermore, turbulence coexists with laminar flow i.e. the flow is intermittent. In practice, there can be a third threshold Re_t which signifies the point above which the entire flow is turbulent, where $Re_g < Re_t < Re_c$. The range between Re_g and Re_t would then be the *transitional range*. In brief, turbulent transition is sub-critical, thus, must be triggered by finite size perturbations and is characterised by spatio-temporal intermittency.

In fact, intermittent turbulence had already been observed by Reynolds [10] in his experiments on pipe flow when he reported the appearance of *flashes* of turbulence before the flow turned fully turbulent. Linear stability and hence sub-critical transition is an important premiss for such a behaviour. Indeed, all evidence suggests that laminar pipe flow is linearly stable for all Reynolds numbers i.e. $Re_c = \infty$ [12, 13]. Hence turbulent transition can only be triggered by a finite size perturbation and laminar flow can, in theory, be sustained up to arbitrarily large Reynolds numbers. In practice, Pfenninger [14] managed to keep pipe flow laminar up to $Re = 100,000$, taking extreme care to suppress any background disturbances.

Reynolds' turbulent flashes were investigated in detail by Wygnanaski *et al.* [15, 16] who defined what is known as a *turbulent puff*. It denotes a localised patch of disordered motion that, on average, has a constant length at a given Reynolds number. It has been shown that these puffs decay following a memoryless process, with the mean lifetime before decay increasing with Reynolds number [17]. Moreover, Avila *et al.* [18] found that the mean lifetime before splitting also follow a memoryless. In this way they determined what they called the *critical point*, Re_g . At this Reynolds number the turbulent fraction i.e. the fraction of the length of the pipe occupied by the puffs can theoretically be sustained for ever in an infinitely large system.

Spatio-temporal intermittency is also observed in turbulent transition in plane flows. Since these flows also extend in the span-wise direction, the geometry is essentially two-dimensional. In this case, intermittent turbulence manifests in the form of coherent structures, called turbulent spots which were first observed in boundary layers by Emmons [19]. Similar spots were also observed in Taylor Couette flow (TCF) [20], plane Couette flow (PCF) [21, 22]

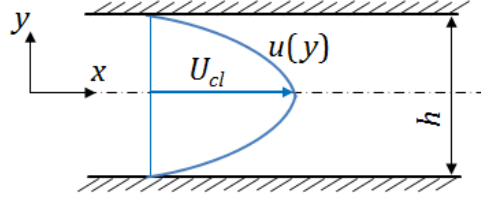


Figure 1.1: Schematic of a plane Poiseuille flow.

and plane Poiseuille flow (PPF) [23]. Comparing these shear flows, it becomes apparent that rather little is known about PPF which might be attributed to complications building large experimental set-ups and the advection due to which turbulent spots can only be observed inside the channel for a short time. Hence, most experiments are performed in PCF and TCF.

The focus of this work is on plane Poiseuille flow, which denotes a pressure driven flow between two stationary parallel plates (see Fig. 1.1). In this case the flow velocity is given by Equ. 1.1 and the centre line velocity relates to the mean velocity by $U_{cl} = 3/2U_b$ [24].

$$u(y) = -\frac{1}{2\mu} \frac{dp}{dx} \left[\left(\frac{h}{2} \right)^2 - y^2 \right] \quad (1.1)$$

In the following paragraphs some notable findings on turbulent transition in PPF are reviewed. As previously explained, transition to turbulence is sub-critical and finite amplitude perturbations are necessary to trigger turbulence. All this happens below the *unconditional* threshold which in the case of PPF is $Re_c = 7696$ [25]. In particular, localised perturbations, e.g. triggered by fluid injection, grow into spot-like turbulent structures surrounded by streaks and waves.

Even though the Reynolds number always compares inertial to viscous forces, different characteristic length and velocity scales might be used. In particular, in PPF a range of slightly different definitions is used. In this work, only the mean Reynolds number $Re_m = U_b h / \nu$ is used, based on the bulk velocity and the full channel height. In contrast, various authors also use the $Re_{cl} = U_{cl} \delta / \nu$ where U_{cl} is the centre line velocity of the laminar flow and

$\delta = h/2$ the channel half-height. In addition, some authors also use $Re_\tau = u_\tau \delta \nu$ where u_τ is the friction velocity. These definitions relate to each other as follows: $Re_m = 4/3 Re_{cl}$ (e.g. $Re_{cl} = 1000$ corresponds to $Re_m \approx 1330$); for Re_τ the conversion is ambiguous since Tsukahara *et al.* [26] define it in a way, such that Re_τ varies with the size of the computational domain. However, for the range of Reynolds numbers covered in this study $Re_m \approx 27 Re_\tau$ (e.g. $Re_\tau = 56$ corresponds to $Re_m \approx 1500$).

Carlson *et al.* [23] who studied turbulent spots in detail using a flow visualisation technique, found that these structures had an arrowhead shape pointing in stream-wise direction and longitudinal streaks around their back. In the centre, fine scale turbulence was observed whereas oblique waves delimited the front and the wing tips. Carlson *et al.* also suggested that spots would eventually split into two while the flow in the middle of the channel would re-laminarise. They could not trigger growing spots repeatedly below $Re_m = 1330$. Alwayoon *et al.* [27] mostly confirmed these findings but reported that they could not even trigger any spots below $Re_m = 1470$. However, they were only interested in high-Reynolds number spots that developed into cohesive structures.

It is important to note that the velocity field inside of the spot has the same characteristics as a fully developed turbulent flow at low Reynolds numbers. This was confirmed by Klingmann and Alfredsson [28] through hot-wire measurements. Furthermore, they stated that there was a minimum threshold for the initial perturbation below which no turbulent patch was triggered. Conversely, the turbulent spot was independent of the initial amplitude for perturbations above the threshold.

Up to this moment, the sole focus lay on turbulent spots. Yet, Tsukahara *et al.* [29] introduced the idea that intermittent turbulence manifested as a periodic stripe pattern. In particular, they had performed Direct Numerical Simulations (DNS) of a fully developed turbulent flow while decreasing the Reynolds number in small steps. They observed the formation of oblique bands eventually filling the whole width of their periodic domain. These bands consisted of stream-wise streaks that were intermittently disturbed by areas of stronger turbulence. This resulted in an alternation of quasi-laminar

and turbulent flow in the stream-wise direction. They claimed that this stripe pattern was the equilibrium structure of intermittent turbulence in channel flow, in analogy to the equilibrium puffs in pipe flow, that had been studied by Wygnanski *et al.* [16]. For $Re_m = 2300$, these turbulent stripes were advected at the bulk velocity and were inclined by 24° to the stream-wise direction. Hashimoto *et al.* [30] confirmed these findings experimentally when observing the development of grid turbulence. They found a stripe pattern in the range from $Re_m = 1700$ to 2000 . For lower Reynolds numbers they reported that no stripes but only spot-like patches were maintained while all turbulence decayed below $Re_m = 1300$. Later Aida *et al.* [31] numerically studied the development of a localised perturbation in a gigantic computational box ($365h \times h \times 180h$). At the beginning they observed the same development as had been reported by Carlson *et al.* [23]. However, instead of splitting into two spots, the perturbation developed into a V-shaped structure which eventually becomes a stripe pattern of quasi-laminar and turbulent regions. The same development was also observed for PCF by Duguet *et al.* [8]. This showed that turbulent stripes also emerge with increasing Reynolds number.

Seki and Matsubara [32] performed hot wire measurements on re-laminarising grid turbulence in order to determine the transitional range. Measuring the turbulent fraction they found that transition took place between $Re_m = 1400$ and 2660 . They also measured the large scale flow around turbulent structures and explained its origin with the increase of skin friction in turbulent areas.

Tuckerman *et al.* [33] did numerical simulations of turbulent stripes, imposing an angle of 24° in a very narrow, inclined domain. They investigated Reynolds numbers between 1070 and 2530 and found that the relative velocity of the stripe decreased with Reynolds number.

In addition to previously reviewed findings on PPF, it is instructive to compare those with observations on PCF. In particular, the fact that intermittent turbulence develops into stripe patterns underlines the similarity between both shear flows. Moreover, it was proposed by Waleffe [34] that two superposed PCFs would be similar to PPF.

For instance, Barkley and Tuckerman [35] studied PCF numerically in a computational box of minimum size, reporting about three distinct types of

patterns, ranging from uniform turbulence over the intermittent state to laminar flow. They later stated the same fact more precisely by talking of uniform, intermittent, periodic and localised turbulence [36]. They also investigated stripes inclined at various angles to the stream-wise direction. Stable stripe patterns could be obtained in the range from 15° to 66° .

Duguet *et al.* [8] performed DNS for PCF in a large domain, using a heavily disturbed flow field as initial condition at a Reynolds number in the transitional range. At first, they observed decay of the perturbation except for some localised patches at random locations which developed into turbulent spots. These spots grew obliquely and ultimately formed stripes. At what they conclude to be the critical point (Re_g), these stripes don't have a unique angle but existed over a range of $36^\circ \pm 10^\circ$ to the stream-wise direction. For higher Reynolds numbers the stripes would approach an angle of 24° . They also simulated the development of a localised perturbation in a fully laminar flow. This confirmed that stripe patterns could not only result from merging spots but could also grow from a single seed. When starting from a localised perturbation, stripes developed at various angles from 24° to 57° but they cannot be sustained when they are orthogonal (90°) to or in stream-wise (0°) direction. Finally, they pointed out that the smallest initial perturbation was needed to trigger stripes with an angle of 40° .

Duguet and co-workers [37] also proposed a stochastic model for the span-wise growth of turbulent structures in PCF, by creation or annihilation of streaks but also noted the existence of a deterministic regime at low Reynolds numbers. Investigating the laminar-turbulent interfaces Duguet and Schlatter [38] stated that these streaks were advected by the flow whose velocity depended on the wall-normal position. Hence the direction of the interface depended on the stochastic process of streak production which explains why the stripe's angle is not unique but has a continuous distribution.

1.4 Outline

In the first part of this thesis, the experimental set-up and the methodology applied in the measurements is described. In particular, this chapter contains the

description of a novel perturbation technique developed during this project. In addition, a description of the flow visualisation technique and image processing is presented.

Secondly, the results are presented. They are organised in the logical order following the decisions taken during this work as a consequence of preliminary results. Discussions can be found in every section right after the results. Most of this part is dedicated to the description of coherent structures, turbulent spots and stripes, in PPF. An estimate of the critical point for sustained turbulence is also estimated at the end.

Final conclusions are put separately at the end of this thesis. They summarise the comments made in the discussions and underline the most important findings.

Chapter 2

Methodology

2.1 Experimental Set-Up

Experiments on the transition to turbulence in plane Poiseuille flow (PPF) are conducted in the rectangular channel, shown in Fig. 2.1. It is composed of two glass plates, sandwiched together with brass spacers which constitute the lateral walls. Everything is held together rigidly by aluminium clamps placed on both sides with a regular spacing (not shown in the sketch). The channel has a full height $h = 2$ mm. Then the width is as $L_z = 125h$ and a length $L_x = 1000h$.

Fig. 2.1 also shows two LED light bars that are installed next to the channel. Together, they cover a total length of 165 cm. Furthermore three cameras are installed at a height of 150 cm above the channel. They are held by a rail and can be moved to any position along the channel.

The standard coordinate systems has x , y and z in stream-wise, wall-normal and span-wise direction respectively, where x and z are in the horizontal plane and y in the vertical direction. The x -axis is centred in the channel with respect to the span-wise and vertical direction. The origin of the coordinate system is the point where the localised perturbations are injected into the flow (see section 2.2.1). Typically, this is 50 cm away from the main entrance. Normally, dimensionless variables are used. x^* and z^* denote the respective coordinate non-dimensionalised by the gap width h ; the time is given in advective units

$$t^* = tU_b/h.$$

Water is used as a working fluid in a gravity driven flow where the pressure head of the reservoir is approximately 12 m, which is maintained constant to within 1 cm. The water is conducted through 1 inch-pipes and in all sections of the water circuit, the Reynolds number is high enough to assure a well-established turbulent flow, far above the transitional range. Hence, the largest part of the pressure drop up to the channel exit occurs in these pipes. This is important since the hydraulic resistance of the channel fluctuates as a consequence of the intermittent flow. However, if these fluctuations are small compared to the resistance of the whole system, they are negligible and thus the flow rate can be maintained nearly constant in spite of a varying fraction of turbulence in the channel. Before entering the channel, the flow passes through a manual control valve which is used to adjust the flow rate and subsequently through a magnetic flow meter (model *COPA-XE DE23*, fabricated by *ABB*) that measures the flow rate.

In Fig. 2.1 the water flow is indicated by blue arrows. Before entering the channel, the water is divided over four pipes which enter into a settling chamber from the rear. The water has to flow around a plate which is installed in the middle of the settling chamber and acts as obstacle for the four turbulent jets entering from the rear. These features are built in to provide an entrance flow that is approximately uniform over the span-wise width. Then the flow is straightened when it is forced through honeycombs. The cells have a diameter of 6 mm and a length of 50 mm. They are followed by a fine grid with an aperture of 1.2 mm and a wire diameter of 0.3 mm which breaks up the largest remaining eddies. Then the flow is accelerated in a straight convergent of length 100 mm with a contraction ratio of 44.

Along the centre line of the bottom plate of the channel, pressure tappings are installed at several locations. For measurements of the pressure drop, a sensor (model *DP45-14* with membrane *6-28*, manufactured by *Validyne*) was connected to two pressure tappings. It has a full scale accuracy of $\pm 0.25\%$ which corresponds to a global error of ≈ 1 mbar.

According to Schlichting [24], the development length for laminar channel flow is estimated from Equ. 2.1 to be $< 100h$ since the range of Reynolds

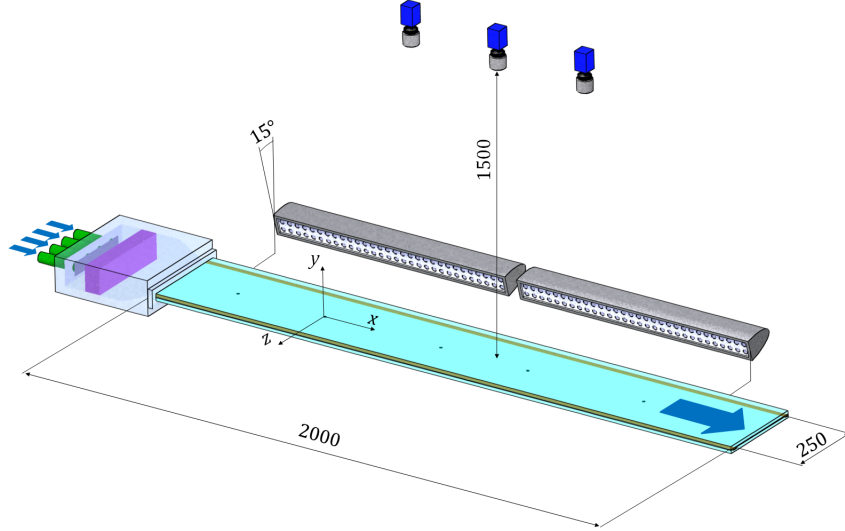


Figure 2.1: Experimental set-up. The honeycombs are shown in purple.

numbers studied in this experiment $Re_m < 2000$. The channel exit is open to the ambient atmosphere and the flow falls into a reservoir from where it is pumped back into the supply reservoir to complete the circuit. The temperature of the water is measured inside this exit flow with a Pt100 probe.

$$\frac{L_e}{h} = 0.05Re_m \quad (2.1)$$

2.2 Perturbation method

In this work the transition from a laminar to a turbulent flow is investigated. For this purpose, a so-called single-seed experiment is performed where turbulence grows out of one single nucleus which is surrounded by a perfectly laminar base flow. Since plane Poiseuille flow is linearly stable in the range of Reynolds numbers investigated [25], this seed must be a perturbation of finite amplitude. Ultimately, two methods are used to generate locally limited initial perturbations. In addition, a strongly disturbed inlet flow is also used to study its re-laminarisation.

2.2.1 Localised Perturbation

Localised perturbations are triggered by injecting a jet of water into the laminar flow. Pressure tappings are installed at several locations along the centre line of the channel. When connected with a pressurised reservoir they can be used for flow perturbation. It generates a jet of diameter $0.25h$ that is injected in the wall-normal direction. The amplitude can be varied by changing the supply pressure of the reservoir which can be adjusted between 0 and 9 bar compared to a pressure drop in the channel of less than 0.05 bar. The injection is controlled with a solenoid valve (model VA 210-001 fabricated by *Staiger*) with short opening and closing times of ≈ 1 ms. In order to generate a turbulent spot, it is typically kept open for 10 ms (corresponds to 3 advective units).

In this standard configuration (injection time 10 ms), the injected volume as a function of the supply pressure is shown in Fig. 2.2. These measurements were performed by firing the perturbation 200 times in a beaker that was open to the ambient atmosphere. Of course the pressure in the channel is slightly higher but since it is smaller than 0.05 bar, this graph gives a good estimate. Fig. 2.2 shows that the injected volume (≈ 0.1 ml) is always very small compared to the total flow rate ($Q \approx 0.3$ l/s) and, as will be seen later, even negligible compared to the absolute accuracy of the flow rate measurement.

The injection of a jet introduces a complex perturbation into the flow. However, as Klingmann and Alfredsson [28] have shown, the characteristics of the turbulent spot are independent of the precise amplitude if it is larger than a certain threshold. This observations was also made in this experiment, yet only in a statistical sense. The reason is that several distinct pathways of spot development are observed as will be pointed out in section 3.2.

Finally, this method allows to study a single perturbation in a calm environment. Hence it is a very common perturbation technique, e.g. used in [23, 27].

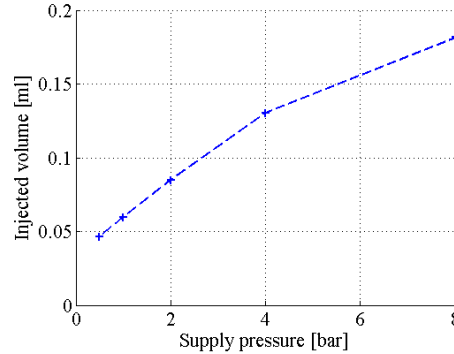


Figure 2.2: Injected volume as a function of supply pressure.

2.2.2 Extended Perturbation

A second method is also used to trigger disturbances. It was specifically developed to produce turbulent stripes at low Reynolds numbers. As will be discussed in section 3.3, finite size effects seem to play an important role in this case. In fact, this extended perturbation covers a much larger area than the localised one. Fig. 2.3 shows a sketch of a novel perturbation mechanism. For better visibility the glass plate on top is partially cut away in the image.

At the origin of the perturbation is an iron sphere which is permanently placed inside the channel. A strong perturbation is brought into the flow when the sphere is set into motion and moves across the channel. The sphere also creates a wake but it decays within $100h$ at $Re_m < 1200$. Due to the wake, this perturbation technique cannot be used at higher Reynolds numbers, but in this range the localised perturbation is effective and can be used instead.

The spherical obstacle is set into motion by sliding a powerful magnet along a rail installed above the upper glass plate. The magnet holds the sphere in place and forces it to cross the channel when a perturbation shall be triggered. This causes a strong, stripe-shaped perturbation. The force necessary to achieve strong accelerations is supplied by a pneumatic cylinder. In this way the magnet is pushed along the rail until it is decelerated violently when it hits a physical stopper that is installed on the rail. Of course, this process, in particular the impact on the stopper, produces enormous vibrations that would be in conflict with the low level of background disturbances needed for

precise measurements on turbulent transition. Hence, the device is isolated from the channel and the frame holding it; no physical contact is made.

In principle, the velocity of the magnet can be adjusted by varying the supply pressure. However, a high pressure is generally preferred for two reasons: firstly, convection plays a minor role if the magnet moves at a higher velocity such that there is tighter control of the initial angle of the turbulent stripe; secondly, only a strong driving force that is much larger than the dry friction between the slider and the rail assures that the magnet moves at a relatively constant velocity. In principle, a higher velocity of the sphere also causes a stronger perturbation. Thus, pressurised air with 9 bar is supplied. For this case, the movement of the magnet was investigated by recording the motion with a camera at a frame rate 100 Hz. The result is as shown in Fig. 2.4. The magnet (and the iron sphere with it) reach the terminal velocity after 3 cm (15*h*) only. Moreover, the terminal velocity almost reaches 2 m/s which is considerable faster than the mean flow velocity $U_b \approx 0.5$ m/s. In practice, one observes that this acceleration and terminal velocity are high enough to initiate a highly perturbed flow along a straight line developing into turbulent stripes. This even works in a range of low Reynolds numbers where a localised perturbation is not efficient any more.

Spherical obstacles have already been used to provide a perturbation. For instance, Bottin *et al.* [1] used a stationary bead as a point-wise perturbation in a plane Couette flow. They pointed out that the perturbation introduced by the spherical obstacle was similar to the disturbance by a thick wire. This suggests that a rapid motion of the sphere might cause a similar perturbation as a long cylindrical obstacle that is lifted into the channel for a short moment.

2.2.3 Disturbed Inlet Flow

In both previously mentioned perturbation techniques, a spatially limited disturbance is put into a laminar base flow in order to study its expansion or decay. In contrast, this third method disturbs the entire flow close to the inlet. Hence, the base flow is not laminar but heavily perturbed. At low Reynolds number the disturbed inlet flow calms down to the laminar state

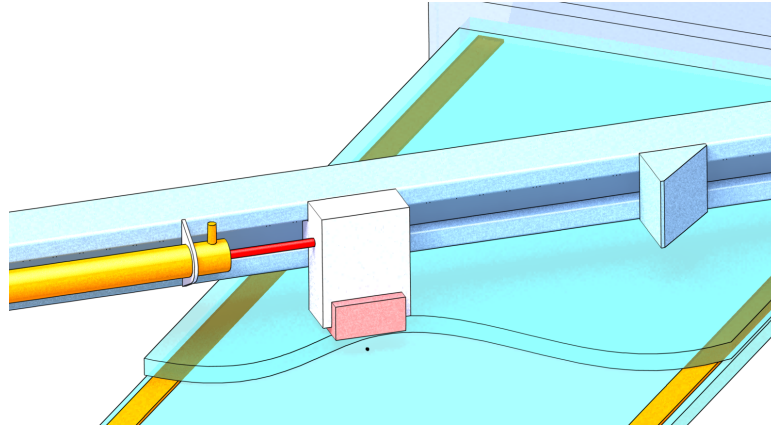


Figure 2.3: Triggering mechanism.

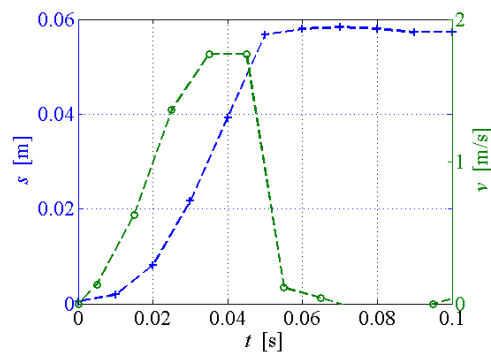


Figure 2.4: Velocity of the extend perturbation mechanism vs. time.

further downstream. However, in the transitional range a finite amount of the initial perturbation should persist and the remaining seeds are expected to grow into new structures such as turbulent spots or stripes.

A disturbed inlet flow is achieved by placing obstacles close to the entrance of the channel. Two rectangular plates of size $70 \times 40 \times 1.5$ mm are used. The perturbation originates from flow separation around sharp corners of the plates and the disturbance is enhanced by the local increase of the Reynolds number due to partial blockage of the channel. In principle the strength of the initial disturbance varies as a function of the relative orientation of the plates inside the channel. However, it is almost impossible to estimate the strength of the perturbation which is the largest disadvantage of this method.

This technique is conceptually similar to experiments like [30, 32] where a turbulence grid was used at the channel inlet. The unknown size of the perturbation is inconvenient. However, it shall be used to compare with the results from the other two perturbation techniques.

2.3 Flow Visualisation

The main focus of this work is on the development of perturbations inside the channel. In particular, their size and shape is investigated which makes it necessary to observe the flow in a large part of the channel. Flow visualisation is found to be the most suitable measurement technique. For this purpose platelet shaped mica particles are used (product name *Iriodin 9103*, fabricated by *Merck Millipore*). Their size ranges between 5 and 40 μm and their coated surface reflects light specularly.

With a relative density of around 3 g/cm^3 , the particles are considerably heavier than water. However, the flow velocities in the channel are relatively high ($U_b \gtrsim 0.5 \text{ m/s}$) and thus the residence time in the channel is short. Consequently, particles are not likely to settle but to follow the flow sufficiently well to visualise the features of intermittent turbulence. Additionally, the 3D flow is not of interest since only 2D flow structures are investigated. All in all, the properties of these particles are judged sufficient for the purpose of the experiments performed.

The flow visualisation technique employed in this experiment is based on the fact that platelet shaped particles align with the flow, the normal to the platelet surface pointing into the same direction as the gradient of mechanical strain. If the channel is lighted from a single source, the amount of light that is reflected towards the observer, the brightness, depends on the inclination of the particles. In particular, in a laminar flow the surface of every platelet is aligned with the channel such that it has a uniform brightness.

In contrast, if the platelets align with the fluid motion in a turbulent flow, the inclination of the platelets changes in space and time. Since the inclination of the platelets is related to the brightness, the flow is coloured in different shades of grey which allows to distinguish the shape of turbulent eddies or other flow patterns. Carlson *et al.* pointed out that these platelets thus visualise the vorticity field [23].

In this work the channel is continuously lighted from one side of the channel. In total, 120 high power LEDs with a 30°-spot beam and a total luminosity of 14,000 lm illuminate the entire length of the channel sufficiently. Uniform DC current is provided in order to avoid high frequency flickering of the LEDs. The light source is placed at an angle of 75° from the vertical. The cameras are placed at a height of 150 cm right above the channel. In this configuration, laminar flow looks dark on the images, whereas areas of higher vorticity are lighter. For better contrast the bottom plate of the channel is covered with black paper.

The cameras (model *acA2040-180km*, fabricated by *Basler AG*) have a resolution of 2048 × 2048 px and can reach a maximum frame rate of 180 frames per second. They are connected to the computer via the serial communication protocol *Camera Link*. The process of taking an image is controlled via TTL pulse. This allows a precise timing with respect to the triggering of the perturbation. The cameras are used with a standard *Nikon* lens (model *AF Nikkor 50mm f/1.8D*).

The cameras are used to record grey scale images at the maximum resolution (2048 × 2048 px). In this case, one camera can cover approximately an area of 34 × 34 cm². In order to capture the instantaneous flow field, a high shutter speed of 1/400 s was chosen.

2.4 Image Processing

In this experiment, turbulent spots are solely monitored visually and the data is only recorded in form of images captured by the cameras. Hence information has to be extracted from the primary data through image processing. In order to measure the size (area and span-wise extent) of the turbulent structures observed in experiment, a self-developed MATLAB code automatically performs the following steps:

- In all images the background is suppressed by division. In contrast to subtraction, division also takes non-uniform lighting into account.
- A global threshold is applied, setting all pixels whose luminosity is below a certain value to zero. In particular, this is done to distinguish relaminarised flow from the turbulent structures. Since the global brightness varies considerably with the amount of particles in the water, this value has to be adjusted for every round of measurements. In practice, this value has to be slightly higher than the general brightness of the background. The threshold is increased in small steps and in short test runs the user has to check that no turbulent structure are wrongly suppressed.
- Noise is removed by neighbourhood averaging. In practice, the best result is reached when using a spatial average, weighted by a Gaussian bell-curve [39]. Hence a rotationally symmetric Gaussian low-pass filter is used. A standard deviation between 2.5 and 3 is found to give the best results.
- The entire domain is chopped up into sub-areas and the spatial standard deviation of pixel luminosity is calculated for each one of them. Ultimately, coherent structures are detected by applying another threshold on this standard deviation. The sub-areas are chosen to be 32 px long (in stream-wise direction) and 16 px wide. The reason is that the perturbation is expected to be partly composed of from longitudinal streaks. Their presence would increase the standard deviation in a rectangular area such as the one proposed.

- Since large coherent structures are investigated, the processing is finished by smoothing the interfaces using a technique called erosion and filling the holes in order to find the area of the structure. This step is based on the experience that there are no holes in the structures observed.

2.5 Error Estimates

In this work, experimental data is solely extracted in the form of photos and the information is put into context by comparing with the *a priori* single control parameter Re_m . Therefore, measurement errors may arise from the camera timing and the evaluation of the Reynolds number, using the flow meter and temperature measurements.

First, the cameras are triggered automatically and the timing is precise to less than 1 ms. In addition, the exposure time is $1/400 \text{ s} = 2.5 \text{ ms}$. This is less one in the advective time scale and negligible when compared to observation times of $O(100)$.

Secondly, the accuracy in the measurement of the Reynolds number depends on the geometry of the channel as well as the flow rate and temperature measurement. Since $Re_m := U_b h / \nu = Q / (w \nu)$, small variations of the channel height along stream-wise direction have no influence on the Reynolds number. Curvature in the walls would obviously disturb the flow but since the channel is made of strong glass plates (thickness 10 mm) deformation under its weight or the water pressure are negligible compared to other inaccuracies. Conversely, changes in the span-wise channel width add up to the global error in the Reynolds number. The lateral walls are aligned to within $\pm 1 \text{ mm}$ which corresponds to an error in Re_m of 0.5 %.

The flow is gravity driven and the pressure head varies by less than a centimetre compared to a total head of approximately 12 m. Hence the flow rate can be assumed to be approximately constant. The magnetic flow meter, however, has an accuracy of $\pm 0.5 \%$.

The temperature of the water increases continuously during one experimental run, mostly due to mechanical dissipation. However, the water is cir-

culated for several minutes before starting the experiment. Thus, the water is well mixed and the temperature is approximately uniform such that the variations are small and continuous measurement of the Reynolds number can be kept within a range of ± 10 .

The temperature is measured with a Pt100-probe placed in a small reservoir which is installed right after the channel exit. Due to relatively high flow rate, the water in this reservoir is well-stirred and can thus be assumed to be approximately at the same temperature as the channel. Calibration of the temperature probe show that the temperature can be measured with an accuracy of $\pm 0.1^\circ\text{C}$. From the temperature measurement, the kinematic viscosity is calculated using a forth order polynomial approximation. At an operating temperature of $\approx 25^\circ\text{C}$, the error in the temperature reading corresponds to an error in Reynolds number of 0.2 %.

Moreover the viscosity is modified by the presence of the particles used for flow visualisation. Since, the particles are much smaller than the characteristic length of the channel, Einstein's formula is used to estimate the effective change in viscosity $\nu_{\text{eff}}/\nu = 1 + 2.5\phi$ where ϕ is the volume fraction of the particles [23]. For 250 g and ≈ 50 L of water this gives $\nu_{\text{eff}}/\nu \approx 1.005$.

Considering all these effects, it can be concluded that the Reynolds number in the range of measurements is $Re_{\text{eff}} = Re_m \pm 10$.

Chapter 3

Results and Discussion

3.1 Properties of the Channel Flow

3.1.1 Transition to Turbulence

In the experimental set-up used, the channel flow remains laminar up to $Re_m \approx 1600$. Above this threshold perturbations (side-wall bound turbulent patches) are triggered randomly on the sides of the channel inlet. This is a result of the sharp edge between the convergent section and the channel.

Single seed experiments can be performed up to $Re_m \approx 1550$ if care is taken to minimise the background level of vibrations. This range is sufficient since the scope of this study is on turbulent spots and stripes at low Reynolds number.

3.1.2 Pressure Drop

Due to the narrow gap width ($h = 2$ mm), measurements of the velocity profile using, for instance Particle Image Velocimetry would be very complicated. Therefore, the pressure drop was measured instead, to check the quality of the experimental set-up.

For each measurement point the temperature, the pressure and the flow rate were averaged over one minute. Three sets of measurement are performed. The first and the second measurement series of the pressure drop are taken

3. RESULTS AND DISCUSSION

over the upstream half of the channel, stretching across $\Delta x = 700$ mm from the uppermost pressure tapping to the middle of the channel, the third one over the downstream part of the channel over a length of 950 mm, reaching from the middle to the last pressure tapping. The measurements show that the pressure drop in the laminar channel flow is approximately 35 mbar for $Re_m = 1500$. In Fig. 3.1 the results for the pressure drop are represented in terms of the Darcy friction factor f .

$$f := \frac{4h}{U_b^2 \rho} \frac{\Delta p}{\Delta x} \quad (3.1)$$

For plane Poiseuille flow the theoretical value of the friction factor scales as follows:

$$f = \frac{48}{Re_h} \quad (3.2)$$

Firstly, both measurements in the upstream half of the channel are in good agreement with the theoretical curve and with each other. This demonstrates the repeatability of these pressure measurements as well as the establishment of fully developed laminar plane Poiseuille flow in the upper half of the channel. This also suggests that 200 mm are sufficient as development length for the channel.

Secondly, the measurements in the downstream part are also reasonably close to the theoretical values. This indicates that the influence of the lateral boundaries does not grow significantly over the length of the channel. In addition, it was seen that turbulent patches started occurring randomly above $Re_m \approx 1600$. However, these spots are small and don't change the static pressure drop significantly, as can be seen in Fig. 3.1.

Finally, it is notable that the difference between the empirical pressure drop and the corresponding theoretical value is less than 0.5 mbar for all measurement points. Moreover, all points of one set of measurements are off the theoretical curve by approximately the same pressure difference. This suggests that they are caused by a calibration error.

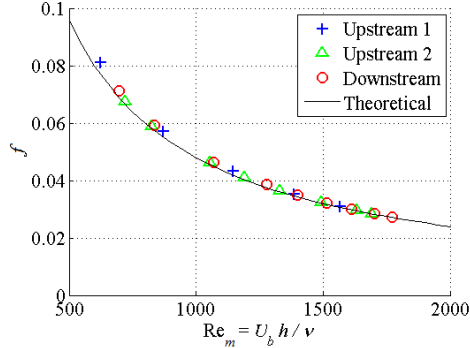


Figure 3.1: Friction factor f .

3.2 Characteristics of Turbulent Spots

3.2.1 Typical Development of a Turbulent Spot

In a first round of measurements, the localised perturbation by fluid injection as described in section 2.2.1 is used to trigger turbulent spots. The development of a typical turbulent spot in time is shown in Fig. 3.2. In this case, the Reynolds number is 1300. The flow is perturbed at the time $t^* = tU_b/h = 0$ in the location $x^* = x/h = 0$, $z^* = z/h = 0$ where a small amount of fluid is injected over 10 ms at a pressure of 0.5 bar.

The first image shows the turbulent spot just after its creation. Waves are visible around the wing tips and stream-wise streaks are trailing from its back. In the centre, one observes that the streaks are disordered and not as bright as around the trailing edge. This corresponds to small scale turbulence.

By comparison of the first and the second image, one observes that the spot grows in both the stream-wise and span-wise directions. Some waves are still visible around the wing tips. In proximity to these waves two areas of small scale structures are present whereas the centre of the spot calms down, yet still contains several streaks. In contrast, the area of the former leading edge has fully re-laminarised and consequently the spot grows into a V-shape.

Up to this point, observations are fully in line with the results by Carlson *et al.* [23]. They suggested that the spot was just about to split into two. However, the third image shows the same turbulent spot further downstream: all streaks

have disappeared from the centre but instead of splitting into several spots, the disturbance structure develops into two stripe-like structures. Just like the initial spot, these stripes have waves around their new leading edges. In the centre, the stripe contains an area of fine structures which is delimited by longitudinal streaks at the upstream side. The stripes are straight and the fine scale area has a clear angle to the stream-wise direction.

It must be underlined that this is only one possible development of a turbulent spot. Since its evolution is stochastic, all spots are essentially different but several categories of pathways can be distinguished. In particular, the spot might only develop one branch independently of the strength of the perturbation. This shows a sensitive dependence on initial conditions. Consequently, only a statistical approach is sensible as previously pointed out by Bottin and Chaté [40] for PCF.

Moreover, the third image shows a relatively large area of re-laminarised flow between the two stripes. One observes that this region originates because longitudinal streaks break off the stripe's trailing edge and ultimately decay. In the image, this is just about to happen for a bundle of streaks separating from the right stripe, in the bottom half of the photo. The growth of a calm flow region in the centre suggests that turbulent stripes only decay but never grow on their trailing edge in the upstream direction, as will be shown later. In the particular case shown in Fig. 3.2 the stripes grows much faster at its leading edge than it is consumed at its rear, which causes a positive net growth of the whole structure.

The development of a turbulent spot is slightly different for higher Reynolds numbers. For instance, Fig. 3.3 shows a turbulent spot at $Re_m = 1500$ in a downstream position that can be compared to the third image from Fig. 3.2. Its wing tips touch the lateral walls but some interesting qualitative observations can still be made. First, it is remarkable that the centre of the flow did not re-laminarise fully (*a* in Fig. 3.3). Its trailing edge is still formed by parts of the original spot, involving both streaks and small scale structures and one stripe growing in positive z -direction is still connected to it. Secondly, it can be seen that both stripes that had grown from the turbulent spot have split (*b*). The word *splitting* shall be used to denote the independent formation of a new

stripe next to an existent one, if both are approximately parallel. As can be interfered from Fig. 3.2, this happens if the original stripe breaks. The mechanism suggested for this process is as follows: a turbulent stripe randomly bends at one location into an S-shape; if the stripe breaks in this location, two parallel pieces of the original stripe exist, one from the trailing edge to the break point and one from the break point to the leading edge. If the rear part now forms its own leading edge, it can form a second stripe that is parallel to the other piece. Now, both, the rear and the front of the original stripe, have individual leading edges where new streaks are seeded into the laminar flow. Hence, they are growing independently from each other and thus form a stripe pattern. The rear part of the original stripe grows on the upstream side of the second one. Finally, new stripes can also form by another process, which shall be called *branching*. In this case the newly seeded stripe grows into the opposite span-wise direction compared to the original stripe. Furthermore, the original stripe does not break but stays intact. One fully formed example, can be seen in the centre of the image (c). Moreover, there are various points where a branching event is just taking place (d). They are marked by a bundle of streaks outside of an existing stripe. These streaks are inclined to the stream-wise direction and form an arrow-head shaped, triangular structure. It is notable that in both cases, splitting or branching the new stripe is always seeded in front (downstream) of the originally existing one.

The flow structure shown in Fig. 3.3 has the same features as simulation results by Aida *et al.* [31] who describe the evolution of a turbulent spot in a V-shape stripe pattern (note that $Re_m = 1500$ corresponds approximately to $Re_\tau = 56$ used in that publication).

Having observed that turbulent stripes can split and branch off, it is reasonable to assume that the stripe pattern of laminar and turbulent areas will finally fill the entire channel. Indeed, Duguet *et al.* [8] reported that a localised perturbation in a PCF ultimately developed into a stripe pattern. The same development could now be observed for PPF. The flow became intermittent, developing into a stripe pattern with both turbulent and laminar flow being present. This intermittent behaviour was also observed by Seki and Matsubara [32] who used hot-wire probe in a re-laminarising flow. However, due to

this measurement technique they were not able to observe the nature of these patterns.

3.2.2 Spreading of the Turbulent Spot

Fig. 3.2 shows that a turbulent spot expands in both the stream-wise and the span-wise direction. This was measured using appropriate quantities that can be defined unambiguously in spite of the random nature turbulent structures.

First, the so-called spreading angle shall be used as a measure for the span-wise growth to assure a simple comparison with other studies. Fig. 3.4 shows a schematic which explains the definition of this quantity: two diverging lines represent the envelop of the turbulent spot in a mathematical sense i.e. they are the trajectories of the spot's wing-tips. These lines define the spreading angle but for conventional reasons only the spreading half-angle is used. The variation of the average spreading half-angle with Reynolds number is shown in Fig. 3.5. Errorbars give the fluctuation in terms of standard deviation. For every measurement point, the average over 30 spots is considered. The spreading half-angle is found to be around 6° in the entire range while it slightly decreases with Reynolds number.

The size of the spreading half-angle is in good agreement with previous findings: Carlson *et al.* [23] reported 8° for $Re_m \approx 1330$ and Alvayoon *et al.* [27] found 6° for $Re_m \approx 1450$. However, in the latter study, an increase of the spreading half-angle with the Reynolds number is mentioned which was confirmed for high Reynolds numbers by Henningson and Alfredsson [41]. Yet, it must be pointed out that these studies looked at much higher Reynolds numbers from $Re_m = 1500$ to 4000 .

Ultimately, the spreading angle is of limited use since turbulent spots do not remain compact patches but develop into stripe patterns. The stream-wise growth gives a better indication of the area covered by intermittent turbulence, as can easily be seen by comparison of the third image in Fig. 3.2 and Fig. 3.3. In order to measure stream-wise spreading of the turbulent spot, the positions of the leading and trailing edge are monitored. They are defined as the most downstream respectively upstream part of the entire turbulent

3. RESULTS AND DISCUSSION

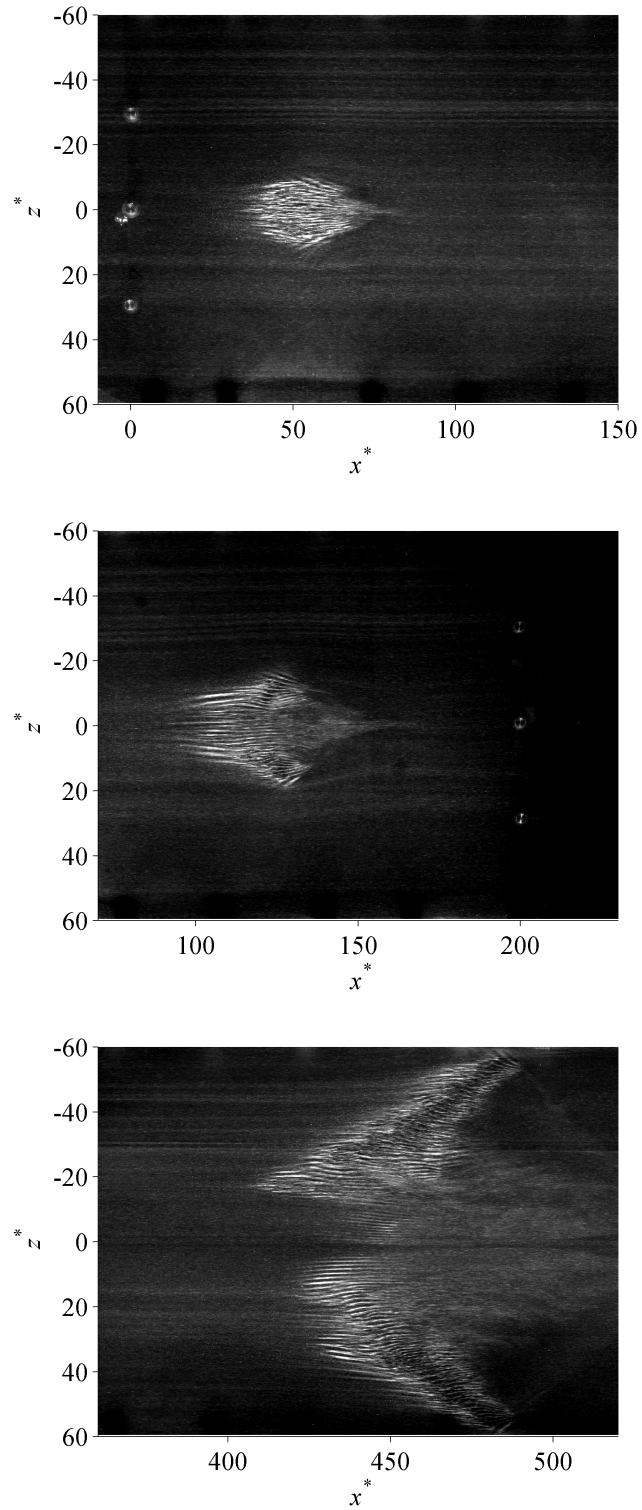


Figure 3.2: Development of a turbulent spot at $Re_m = 1300$. Images are taken at $t^* = 60$ (top), 115 (middle) and 400 (bottom). $x^* = x/h$ and $z^* = z/h$; $x = 0$ and $z = 0$ at the point of perturbation.

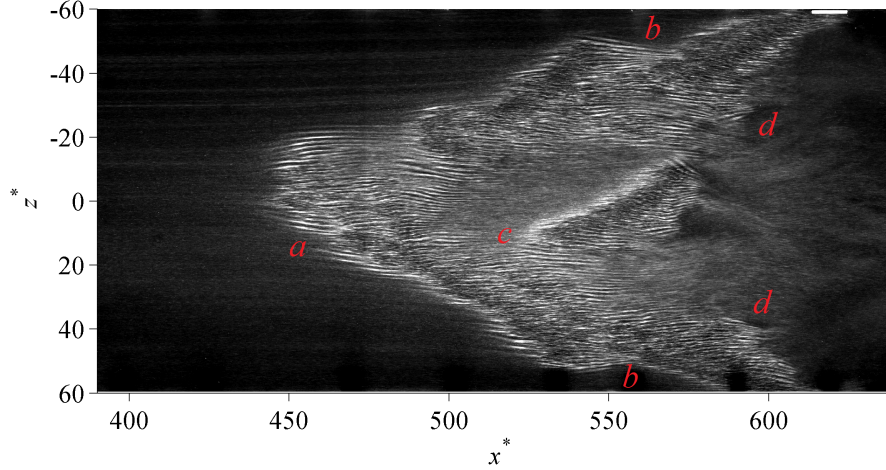


Figure 3.3: A turbulent spot at $Re_m = 1500$, $t^* = 500$.

structure. Whereas the leading edge can be clearly identified, the streaky rear of the spot is ill-defined. Thus, the position is averaged over 30 spots and for better comparability only spots that have developed into two branches (such as seen in Fig. 3.2) are considered. The results are shown in Fig. 3.6 in non-dimensional form. Only the average development is shown here whereas the stripes' growth is inherently stochastic. The fluctuations are of the order of $\pm 5h$; they are slightly larger for low Reynolds numbers. These fluctuations are very small compared to the characteristic size of turbulent structures involved. This could be related to the fact that only spots that had developed into two or more stripes were considered.

For the leading edge, the average trajectories for various Reynolds numbers collapse into a single straight line. This observation is in good agreement with numerical results by Aida *et al.* [31]. First, this suggests that the leading edge of a turbulent spot moves with a constant velocity, if fluctuations are left aside. Secondly, this velocity seems to be invariant with the Re_m . Averaging the data from 3.6, one finds that $u_{LE}/U_b \approx 1.22$ where u_{LE} denotes the stream-wise velocity of the leading edge. Conversely, the average propagation velocity of the trailing edge u_{TE} depends on the Reynolds number. In particular, the propagation velocity of the trailing edge decreases with rising Reynolds number. Consequently the span-wise spreading of turbulent spots is enhanced at

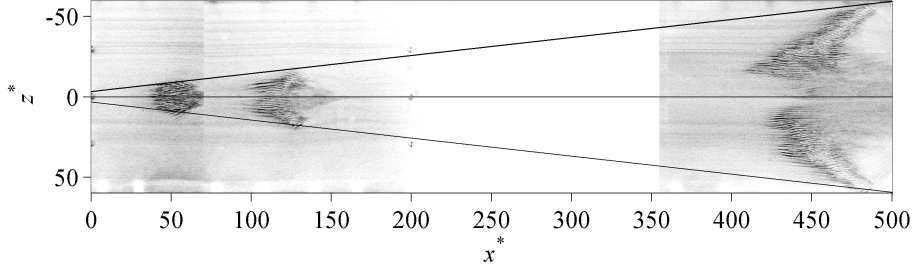


Figure 3.4: Schematic for the spreading angle of a turbulent spot.

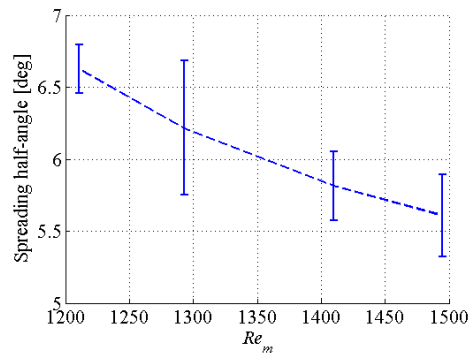


Figure 3.5: Variation of the spreading angle with the Reynolds number.

high Re_m . Finally, it is remarkable that the trajectories of front and rear diverge even for $Re_m = 1200$. This signifies that the net growth of the turbulent spot is positive i.e. it is not decaying. The last observation is particularly interesting since various studies claim that turbulence cannot be maintained at $Re_m < 1300$ [27, 30, 32].

3.3 Growth and Decay Rates

One objective of this work is the determination of a *critical point* for sustained turbulence in plane Poiseuille flow. By analogy to pipe flow, it shall be determined in a single seed experiment following a similar approach as Avila *et al.* [18]. Here, the downstream evolution of the ensemble averaged turbulent fraction is determined as a function of the Reynolds number. Below critical, this value should ultimately decrease downstream, and above it, the turbulent

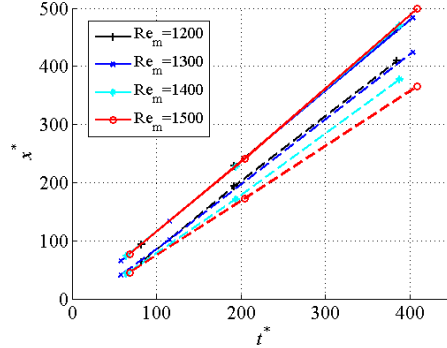


Figure 3.6: Position of the spot's leading (-) and trailing edge (- -) over time.

fraction should increase. Whereas the turbulent fraction in the pipe was measured as the number of turbulent puffs per unit length, the surface area of the turbulent spots is chosen in plane Poiseuille flow.

In a first attempt to describe the growth or decay of intermittent turbulence in a plane Poiseuille flow the average evolution of turbulent spots is investigated. The evolution of a spot is monitored in the following way: Re_m is fixed to within ± 5 and for every Reynolds number a series of data points, consisting of several downstream positions, is recorded. For each individual data point, 100 localised perturbations are triggered and images of them are taken at a single downstream position. Injecting fluid at a pressure of 0.2 bar for 5 ms is found sufficient to trigger turbulent spots in the entire range of Reynolds numbers studied here. Their size is found by image processing as described in section 2.4. The results on the average spot area are shown in Fig. 3.7.

Within the first 100 advective time units, the perturbation spreads out. Only after this initial development time, the influence of the Reynolds number on the growth of the turbulent area is observed. There is a clear and steady growth of the average spot area for $Re_m > 1400$ whereas spots initially decay for $Re_m < 1300$. However, ultimately the average area increases for all Reynolds numbers apart from $Re_m = 1200$.

The reason the initial decay is found when analysing the statistical distribution of the spot size at a given position (Fig. 3.8). Comparing Fig. 3.8a and 3.8b shows the spreading of the localised perturbation. Yet, in most cases, this initial perturbation decays shortly afterwards (Fig. 3.8c). On the other hand, a

couple of turbulent spots are formed which grow in the long term (Fig. 3.8d) in exactly the same way as shown in Fig. 3.2. In the end, these spots dominate the statistics which leads to an increase of the average size.

In addition the same experimental data is presented in an alternative way by showing the probability of decay in Fig. 3.9. A spot is said to decay if its size is less than half the area that was observed at $t^* \approx 55$ (the first measurement point) for the same Reynolds number. The result is found to be independent of the precise value of the threshold. Wiggles that appear in the probability accumulation function for low Reynolds numbers are due to the limited sample size (100).

The main trend is that spots are more likely to decay at lower Reynolds numbers. Yet, in no case, $P_{decay} = 1$ is reached (the maximum is 0.99). In fact, for every value Re_m the probability accumulation function converges towards a finite value < 1 , e.g. $P_{decay} \xrightarrow{t^* \rightarrow \infty} 0.8$ for $Re_m = 1302$. This means that, there is a point in time beyond which spots do not decay any more. This suggests that perturbations following the initial decay have never formed an actual turbulent spot. Conversely, the successful formation of a turbulent spot resulting in a steady growth could be observed in the whole range of Reynolds numbers studied.

Most importantly, this shows that turbulent spots can also grow at Reynolds numbers around 1200, if the perturbation is sufficient to generate a well-formed spot. Moreover, in this range of Re_m it seems that these growing stripes do not stop to grow. However, it will later be discussed later (section 3.4.1) that the developing stripe may grow at its leading edge but also decays at the trailing edge. Even though further studies are necessary, it is already reasonable to assume the existence of an equilibrium between growth and decay at a certain Reynolds number. Thus the existence of a critical point is still justified and its exact value can, in principle, be determined.

In particular, the existence of growing spots signifies that turbulence is maintained. This is in contrast to all previous studies [27, 30, 32] suggesting a critical point of 1300 or above.

Finally, one also notes that a successful perturbation always develops into a stripe-shaped structure. In fact, the compact, round structure of a turbulent

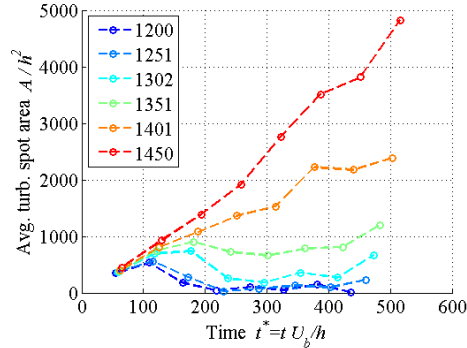


Figure 3.7: Evolution of the average area of a turbulent spot $\bar{A}/h^2 = f(Re_m, t^*)$.

spot cannot persist in time. This suggests that turbulent spots are not the equilibrium form of intermittent turbulence in plane Poiseuille flow. They only exist momentarily after being triggered by a localised perturbation and before growing into a stripes pattern. In this case, turbulent stripes might take over their role as suggested by Tsukahara *et al.* [29].

In a nutshell, the majority of spots triggered by localised perturbation decay at low Reynolds numbers. However, it seems that if a spot develops into a stripe of a certain minimum size, the resulting structure grows most of the time, even at the lowest Reynolds numbers studied here. Conversely, if the spot does not grow into a small stripe initially, it decays. This suggests that the localised perturbation is not optimal way of producing turbulent stripes. Hence, an extended perturbation shall be used in the following experiments.

3.4 Characteristics of Turbulent Stripes

In section 3.2 it was found that localised perturbations trigger turbulent spots which ultimately grow into stripe patterns. Hence, studying turbulent stripes is more significant with respect to the characteristics of spatio-temporally intermittent flow. In particular, it is interesting to see that turbulent stripes seem to grow at Reynolds numbers below 1200, implying that the critical Reynolds number for plane Poiseuille flow lies even lower.

However, section 3.2 also showed that a localised perturbation by fluid in-

3. RESULTS AND DISCUSSION

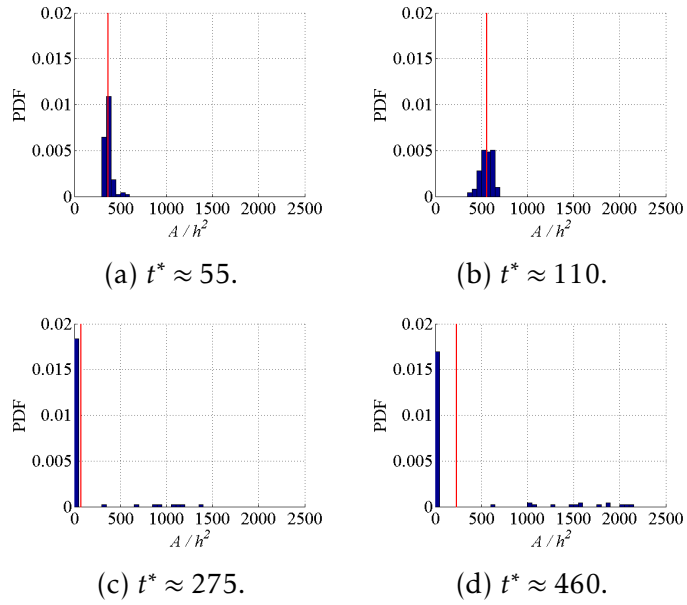


Figure 3.8: Size distribution of turbulent spots at various positions for $Re_m = 1250$. The red vertical represents the average size.

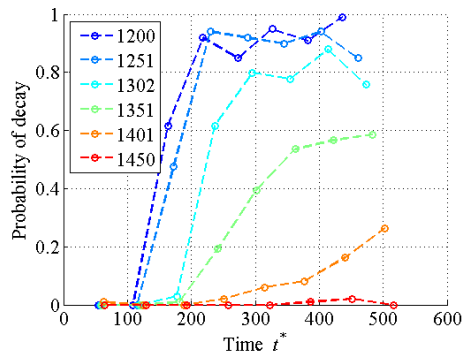


Figure 3.9: Probability of decay for a turbulent spot.

jection is not an efficient method to produce turbulent stripes since only 1 spot out of 100 develops this characteristic shape at $Re_m = 1200$. Hence, a newly developed technique (see section 2.2.2) is employed to produce extended perturbations which favour the development of turbulent stripes.

3.4.1 Typical Development of Turbulent Stripes

The use of an extended perturbation described in section 2.2.2 allows to produce turbulent stripes repetitively at low Reynolds numbers, compared to the thresholds reported in various publications. This is demonstrated in Fig. 3.10 which shows the development of a turbulent stripe at $Re_m \approx 1100$. The extended perturbation mechanism is applied in the area of $-100 < x^* < 0$. The device is inclined to the stream-wise direction by an angle of 50° but due to advection by the flow, the resulting stripe has an effective initial angle of $\approx 40^\circ$.

The first image shows the turbulent strip right after its creation where the wake of the spherical obstacle has not decayed yet. For precise measurement of the growth rate the stripes should only be considered further downstream where they are surrounded by weakly disturbed flow. Thus, the general structure is described with respect to the second and third image: the stripe is composed of stream-wise streaks but the dark centre indicates the existence of small scale motion. The leading edge is wedge-shaped and one can clearly see the waves preceding the main structure of the stripe. By comparison the trailing edge is much smoother and very little small scale motion is found close to it.

A great impression of the typical development of a turbulent stripe can be interfered by comparing the second and the third image. At $Re_m = 1100$, clear net growth can be observed. The leading edge advances quickly and increases the stripes size considerably. Indeed, once a stripe starts growing at its leading edge, it seems that this process does never stop. At least, this has not been observed in the experiment so far. Conversely, the stripe does not expand at its trailing edge but retreats step by step. In general terms, this suggests that turbulent stripes only grow in length at their leading edge.

Indeed, the stripe loses some patches at its trailing edge which separate

and re-laminarise. Notably, this does not happen steadily as in the case of the leading edge but in distinct events that can be described as follows. Even initially, little small scale motion is observed in proximity to the trailing edge. In a first step, this patch of turbulence vanishes leaving behind the longitudinal streaks. These streaks don't stay aligned with the rest of the stripe but bend forward in the stream-wise direction. Finally, this entire patch of streaks cannot sustain itself and decays. The preferred break-point seems to be a location close to the trailing edge where the stripe is not perfectly straight but shows a slight bend. Conversely, this definitely has a stochastic component since several bends observed in the second image did not cause separation but they were straightened out until the third image.

In general, these characteristics of turbulent stripes are consistent with findings about the two branches growing out of the turbulent spot shown in Fig. 3.2. The retreat of the trailing edge gives an explanation for the re-laminarisation in the centre of the turbulent spot. One concludes that the stripes triggered with the extended perturbation qualitatively behave in the same way as the stripes that grow freely from a localised perturbation. Of course, this is also true for the stochastic nature of turbulent stripes due to a sensitive dependence on initial conditions, which makes a statistical approach necessary in order to quantify the development of turbulent stripes.

In general, stripes are straight and slender but their width shows statistical fluctuations. The width denotes the extent of a stripe normal to its length, including fine scale motion and streaks. At high Reynolds numbers, turbulent stripes and the average width is observed to increase from $15h$ to $30h$ in the range $1100 < Re_m < 1450$ but on average does not change in time. This shows the same trend as reported for turbulent puffs in pipe flow [16].

As far as the growth is concerned, one can compare current observations with modelling efforts in plane Couette flow by Duguet *et al.* [37]. They suggested a stochastic growth mechanism behind the creation of new streaks whereas this experiment shows a continuous, steady growth, which might indicate a deterministic growth mechanism. Of course, PCF and PPF are different in the sense that there is no mean flow in PCF. Conversely, in PPF the wedge-shaped leading edge pointing in stream-wise direction seems to play

an important role in maintaining the stripe, in particular, in combination with strong waves originating around the leading edge. This suggestion is based on the observation that all growing stripes share this characteristic whereas they never occur in decaying stripes.

In contrast, the retreat of the trailing edge seems to have a strong stochastic component. The secondary flow around the stripe, which itself is caused by increased wall friction in stripe's area, can be suggested as a reason. In fact, the stripe acts like an obstacle so that a certain amount of the flow takes a detour around its edges. The leading edge is already inclined towards the downstream direction such that this flow has no effect. However, the high velocity flow around the trailing edge causes this part of the stripe to bend forward. Apparently, imposing a much larger angle on the rear of the stripe destabilises it. In section 3.4.3 a reason for this behaviour will be presented.

In addition, Fig. 3.10 also shows several advantages of the new perturbation technique, in addition to the high efficiency in triggering stripes at low Reynolds numbers. Since stripes only grow at the leading edge, they can be triggered with their trailing edge being close to the lateral wall, which effectively doubles the width of the channel as far as the stripe is concerned. Secondly, the stripe-shaped perturbation can immediately form a turbulent stripe. Since no initial development from a spot into a stripe is necessary, using the extended perturbation increases the effective length of the experimental set-up. Finally, the extended perturbation also allows to generate "custom-made" stripes with an arbitrary angle and length. For instance the behaviour of stripes that have not freely grown in their natural angle can be studied in this way. For instance, this allows one to test whether stripes have a preferred angle.

3.4.2 Branching of Turbulent Stripes

For turbulent stripes originating from a localised perturbation, two processes for the formation of new stripes have been observed. A turbulent stripe split into two parallel stripes or branch off, forming a V-shape. The latter process shall be investigated closely. For this reason an image sequence is recorded

3. RESULTS AND DISCUSSION

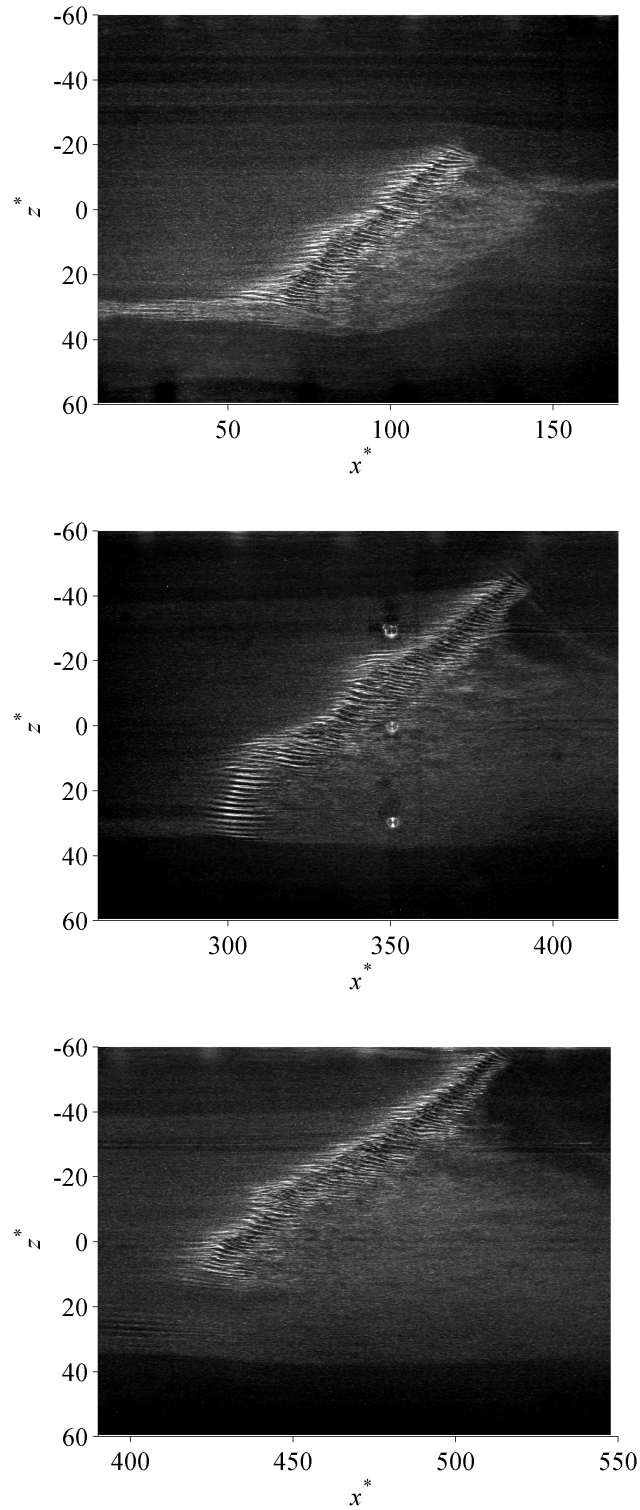


Figure 3.10: Development of a turbulent stripe at $Re_m = 1100$. The photos are taken at $t^* = 170$ (top), 385 (middle) and 480 (bottom). An extended perturbation is applied at $-100 < x^* < 0$.

with a frame rate of 50 Hz (note that the interval between two images, 20 ms, approximately corresponds to $\Delta t^* = 5$), starting at around $t^* \approx 480$. One branching event observed at $Re_m = 1200$ is shown in Fig. 3.11. For this purpose several images are selected from the entire sequence.

The first image only shows the leading edge entering the frame. The stripe has the same shape as in Fig. 3.10 where not branching occurs. Between the first and second image ($\Delta t^* \approx 20$) a pack of four parallel streaks forms at the laminar-turbulent interface, downstream of the stripe, not too far from the leading edge ($z^* \approx 20$). Whereas the streaks in the close neighbourhood are aligned with the stream-wise direction, the front of this pack is inclined towards the leading edge. Until the third image the pack has grown to a size of six streaks. In this moment the streaks closest to the leading edge have detached themselves from the stripe such that the pack sticks out of the front of the stripe. The streaks start forming a wedge shape which seems to have finished by the fourth image. This shape is already similar to the leading edge of the original stripes. Until the last image a stripe has grown to a length of $\approx 10h$. This growth happens by seeding new streaks in the laminar flow in front of the leading edge.

This observation of a branching event underlines the importance of the formation of a wedge-shape leading edge. Branching events don't happen regularly and they are relatively rare at this Reynolds number. In fact, at $Re_m = 1200$ branching could only be observed in the channel with a probability that was of the order of magnitude $O(0.01)$. Notably, splitting such as observed in Fig. 3.3 and resulting in two parallel stripes, was not observed at this Reynolds number. It has only been seen to occur for $Re_m > 1450$ using a localised perturbation.

3.4.3 Natural Angle of Turbulent Stripes

In a next step the inclination of turbulent strips shall be studied. In general, stripes are straight and their inclination with respect to the stream-wise direction is well defined. In this work, the inclination of the stripe will be denoted as α which is defined according to Fig. 3.12a.

3. RESULTS AND DISCUSSION

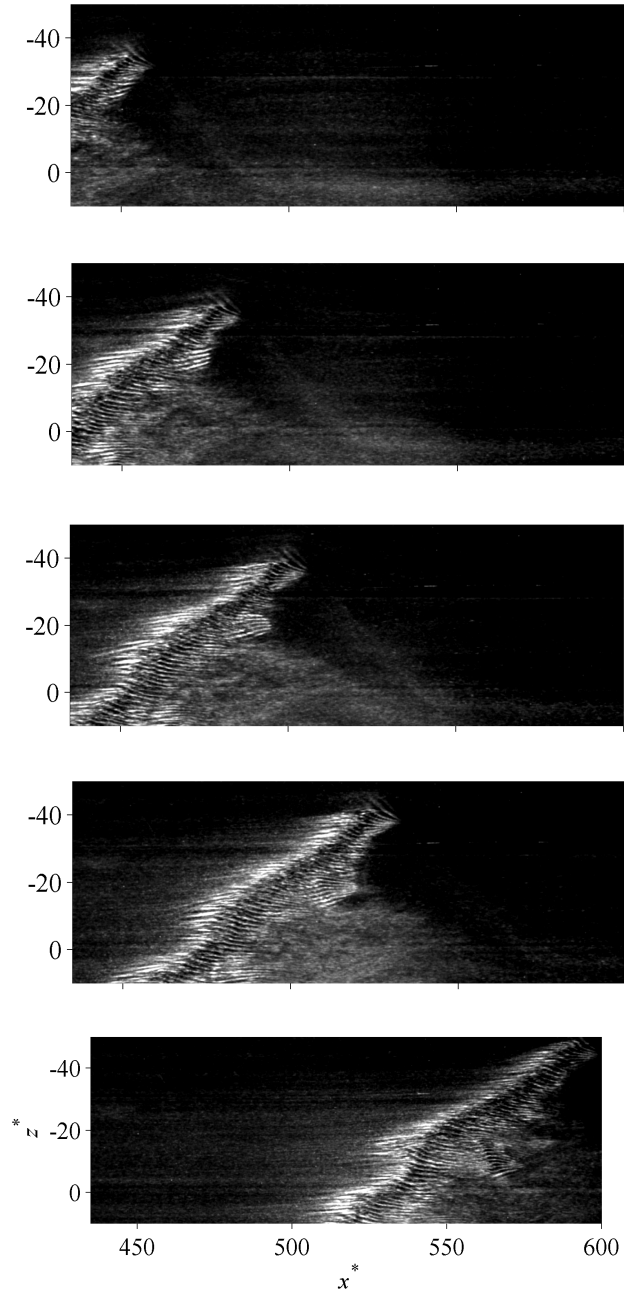


Figure 3.11: Image sequence of a splitting event at $Re_m = 1200$. The time steps with respect to the first image are $t^* = 0, 20, 35, 55$ and 105 .

3. RESULTS AND DISCUSSION

α_{trig}	40°	50°	60°	75°	85°
$\approx \alpha_0$	35°	40°	48°	60°	70°

Table 3.1: Comparison of trigger angle α_{trig} and the effective initial angle α_0 .

In a first test, the time evolution of α is examined after having imposed an initial angle using the extended perturbation method. Fig. 3.12b shows the results for $Re_m = 960$, averaged over 30 stripes. The legend lists the values of the trigger angle α_{trig} . This angle measures the inclination of the triggering device in the laboratory frame with respect to the stream-wise direction. This gives the angle of the trajectory for the spherical obstacle inside the channel. The trigger angle is not equal to the initial angle due to advection by the mean flow. In fact, the initial angle can only be estimated from images showing the stripe shortly after its formation, e.g. at $t^* = 100$. Since these stripes are created by moving the obstacle from the leading to trailing edge, the effective initial angle is somewhat smaller than the trigger angle. The approximate relation between both values is summarised in Tab. 3.1.

Fig. 3.12b shows that irrespectively of the initial angle, the stripes eventually converge towards an angle $40^\circ < \alpha < 50^\circ$. This is an important result since it demonstrates that stripes have a preferred angle and that they auto-correct a wrong angle by converging towards this preferred value. Only after having established these two facts, the existence of a sensible *natural angle* of turbulent stripes can be confirmed.

In a second step the average growth of stripes is measured as a function of the initial angle. Fig. 3.13 shows the time evolution of the average stripe size for a fixed Reynolds number; legend entries give the trigger angle α_{trig} which can be converted to the initial angle using Tab. 3.1.

The growth is measured by two different quantities: the span-wise extent W , as defined in Fig. 3.12a and the area. Fig. 3.13a shows the time evolution of W and 3.13b the evolution of the stripe's area, including the area of small scale motion and the streaks. The time evolution of both quantities only differs in the first stage of development ($t^* < 300$) but eventually both figures show the same trends.

For a trigger angle $\alpha_{trig} = 40^\circ$ and 85° the average size decreases by 25 %

and 50 % respectively, in the time interval $300 < t^* < 450$. This suggests that a large fraction of initial perturbations decay. In contrast, the evolution of the stripes as a function of the trigger angle does not vary much in the range $50^\circ \leq \alpha_{trig} \leq 75^\circ$.

By comparison with Tab. 3.1 one notes that, this range of trigger angles corresponds to the initial angle $40^\circ \leq \alpha_0 \leq 60^\circ$. This is interesting since Duguet *et al.* [8] observed in numerical simulations on PCF that the lowest initial perturbation was necessary to produce a turbulent stripe at an angle of $\sim 40^\circ$. Indeed, it is observed that turbulent stripes cannot be maintained outside this range, e.g. observed in the current experiment for $\alpha_0 = 35^\circ$ and 70° .

Thus, in order to assure the formation of turbulent stripes, it is in the best interest to trigger stripes at an angle that is inside this range. Finally, one notes that this range $40^\circ \leq \alpha_0 \leq 60^\circ$ coincides with $40^\circ < \alpha < 55^\circ$, the interval where the natural angle is expected according to Fig. 3.12b.

For this reason, the natural angle shall be measured in the widest possible range of Reynolds numbers possible with the current set-up. In the end, three different types of perturbations are used in the appropriate range of Reynolds numbers. In every case the perturbation is given enough time to develop into a shape that is as independent as possible from the original perturbation. From Fig. 3.12b one infers that the turbulent spot/stripe needs to develop freely for at least $\Delta t^* > 300$. The angle was detected visually by selecting two points in a straight region of small scale turbulence, such as indicated in Fig. 3.12a. To make sure the values are not biased by decay, deformation or splitting, only well-formed stripes are considered. In this case well-formed means that the angle can be measured unambiguously. Furthermore, stripes that touch the wall are also excluded.

The results of these measurement of the natural angle of a turbulent stripe as a function of Reynolds number are compiled in Fig. 3.14. The set of measurement called “spot” denotes the use of the localised perturbation while providing a supply pressure of 2 bar to the injector; “stripe” stands for the extended perturbation method at a trigger angle $\alpha_{trig} = 50^\circ$; “plate” means the placement of two plates in the channel inlet in order to create a highly disturbed inlet flow. Error bars show the standard deviation at each measure-

ment point. One notes that the results for all three perturbation techniques are consistent since the standard deviation is typically larger than the off-set between different sets of measurements.

In general, the stripe's natural angle α_n decreases with rising Reynolds number over the entire range $900 < Re_m < 1500$. $Re_m = 900$ marks the lowest point where a clear stripe such as previously described could be identified. At this point of very low Reynolds numbers the natural angle is found to be $\alpha_n \approx 45^\circ$. Up to $Re_m = 1300$ the natural angle only decreases slowly but then drops rather quickly to $\approx 25^\circ$.

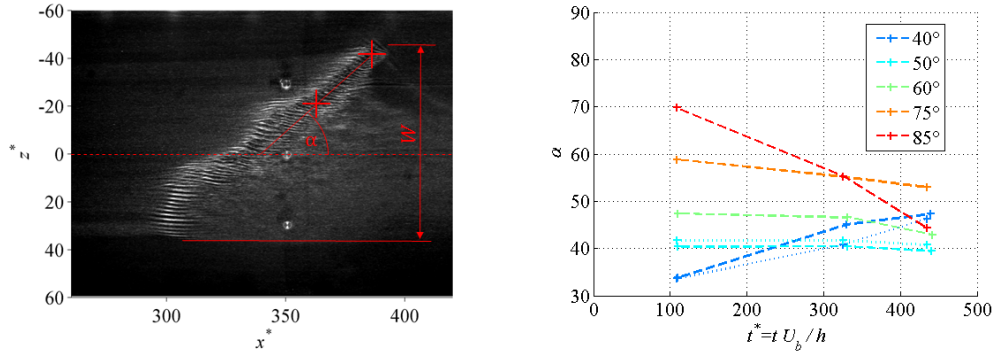
Finally, Fig. 3.14 shows that there is a universal natural angle for turbulent stripes irrespective of the specific perturbation method used. This also adds evidence that the stripes produced from localised and extended perturbation are equivalent. In addition, Fig. 3.15 shows the spread of data for three different points. In every case, a continuous distribution is found suggesting that stripes naturally exist in a certain range around the mean natural angle. Comparing with Fig. shows that this range is identical with the range where the temporal evolution of the turbulent stripes is independent of the initial angle.

The existence of a continuous distribution was also found by Duguet and Schlatter [38] in PCF. The overall range of angles observed $22^\circ < \alpha_n < 47^\circ$ is consistent with results from Tuckerman and Barkley [36]. They enforced the angle in a numerical domain and found that stripe patterns could develop between 15° and 66° . Hence, this should give the maximum stability range for turbulent stripes. The range of natural angles has to be contained but obviously must be considerably narrower. However, having confirmed that the stripe's natural angle varies drastically with Reynolds number, ultimately raises questions about an approach followed by Tuckerman and co-workers [33, 36] who fix the angle of a the stripe over a wide range of Reynolds numbers in a numerical study, e.g. when imposing 24° at $Re_m = 1100$.

3.5 Critical Point in Plane Poiseuille Flow

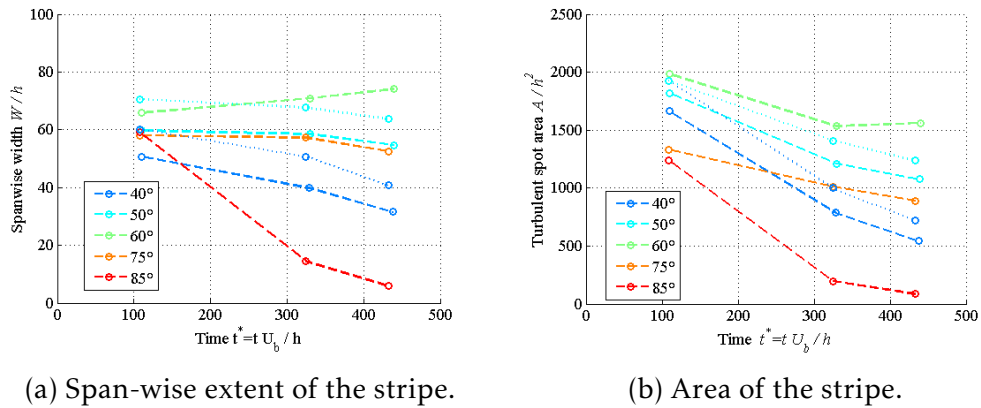
Having established that perturbations in plane Poiseuille flow (PPF) always either decay or develop into a stripe pattern, finally, the critical point shall

3. RESULTS AND DISCUSSION



(a) Definition of the stripe's angle α and the span-wise extent W . (b) Time evolution of the stripe's average angle. $Re_m = 960$.

Figure 3.12: The evolution of the angle of a turbulent stripe.



(a) Span-wise extent of the stripe.

(b) Area of the stripe.

Figure 3.13: Growth and decay of a turbulent stripe as a function of the trigger-angle. $Re_m = 960$.

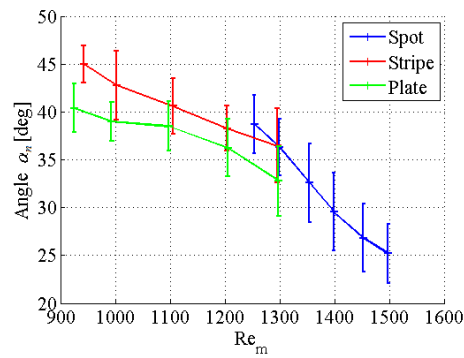


Figure 3.14: The natural angle as a function of Reynolds number.

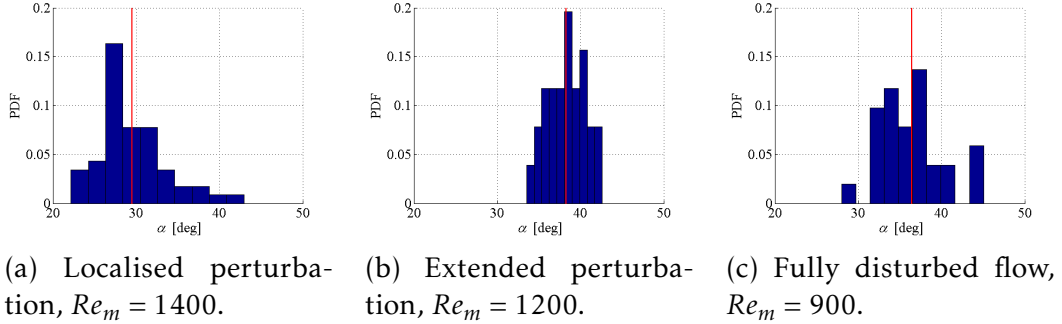


Figure 3.15: PDFs for the distribution for the angle of turbulent stripes. The red vertical represents the mean value.

be estimated. For this purpose, the extended perturbation mechanism is employed while making use of the insight gained into the typical development of turbulent stripe.

At first, the average development of turbulent stripes is investigated. Fig. 3.16 shows the average evolution of the stripes' size. The trigger angle is $\alpha_{trig} = 60^\circ$ (corresponding to an initial angle $\alpha_0 = 48^\circ$), since this lies in the middle of the range where turbulent stripes naturally exist and where the small variations of the initial angle don't influence the formation of stripes. The average is calculated from a sample size of 50.

In a 2D flow, e.g. PPF, the most intuitive way of measuring the turbulent fraction is the area covered by the disturbed flow. However, when performing flow visualisation, the disturbed area of a decaying stripe cannot always be identified unambiguously. The span-wise extent W (see Fig. 3.12a) was found to be a more robust measure for a stripe's growth. Indeed, both measures, the span-wise extent and the stripe's size are equivalent since the stripe has a slender shape with a constant width and its angle is within a narrow range. Of course, this is only true if no splitting events happen, but they were not observed within the length of the channel at very low Reynolds numbers around what is presumable the critical point. Thus, qualitative differences between Fig. 3.16a and Fig. 3.16b only exist in the first interval whereas both measures shows similar results for well-established stripes far from the perturbation.

As for the quantitative measurements, one observes that turbulent stripes

3. RESULTS AND DISCUSSION

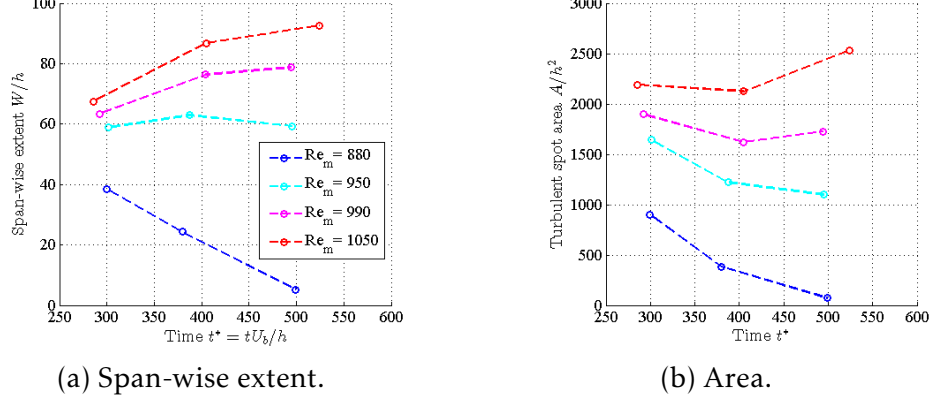


Figure 3.16: Growth of turbulent stripes as a function of Reynolds number. Trigger angle $\alpha_{trig} = 60^\circ$.

on average decay for Reynolds numbers $Re_m \leq 950$. Conversely, there is a net growth of the average size for $Re_m \geq 1000$. This is only possible if a significant fraction of stripes grow. Yet, after a quick rise in size over the first interval, the growth is much smaller in the second interval. This could be related to the beginning decay of the stripe on the trailing edge as discussed in section 3.4.1.

For a trigger angle $\alpha_{trig} = 50^\circ$ ($\alpha_0 = 40^\circ$) the same result is found: the average size grows for $Re_m \geq 990$ and decreases for $Re_m \leq 950$. This is consistent with the results from section 3.4.3 that the behaviour of turbulent stripes is similar as long as their initial angle is within a certain range. In this range of Reynolds numbers, the range of angles is approximately $40^\circ \leq \alpha_0 \leq 60^\circ$.

This suggests that the critical lies in the range $950 < Re_m < 1000$. This is lower than any value reported in earlier publications. Most recently, Seki and Matsubara [32] claimed the critical point to be $Re_m = 1400$. Their estimate is based on the stream-wise evolution of the kinetic energy contained in the velocity fluctuations. However, complete decay for $Re_m < 1390$ is only suggested by extrapolation of their actual data. Furthermore, the hot-wire measurement did not allow them to observe the formation of coherent structures in the same way as this is possible when using flow visualisation.

Chapter 4

Conclusion

In plane Poiseuille flow (PPF), transition to turbulence takes place at Reynolds numbers that are far below the linear instability threshold. Due to its subcritical nature, the transition scenario is characterised by spatio-temporal intermittency which, at low Reynolds numbers, manifests in the form of localised turbulent areas surrounded by laminar flow. In this thesis, a rectangular channel of large aspect ratio and length was used to study the development of these localised structures, in particular, in a lower range of Reynolds numbers than previously considered.

4.1 Summary of the Results

It has long been known that a localised (point-wise) perturbation of sufficient amplitude develops into a turbulent spot of oval shape [23]. Experiments clearly show that these spots develop into stripes forming a V-shape. This confirms numerical results [31] and suggests that *turbulent stripes* are the natural form of intermittent turbulence in plane Poiseuille flow. Conversely, turbulent spots are a transient stage of these localised structures that either decay or grow into turbulent stripes. The formation of these structures has a stochastic nature such that a turbulent spot may decay or as well grow into one or two stripes. For lower Reynolds numbers the probability of decay increases and below $Re_m = 1200$ practically no stripes grow any more.

A new perturbation mechanism for extended perturbations was presented.

4. CONCLUSIONS

The stripes produced with this technique were found to be equivalent to the ones which grow freely from a localised perturbation. Moreover, this method allows for the creation of turbulent stripes at very low Reynolds numbers $Re_m < 1100$.

Turbulent stripes are approximately advected with at the mean flow velocity. Their development also shows a stochastic behaviour. In the range of Reynolds numbers investigated, turbulent stripes are found to grow only on their leading edge. At the same time the trailing edge decays step by step. In general, turbulent stripes grow steadily at Reynolds numbers far below all estimates for the critical point in previous studies. All well-established turbulent stripes which show strong growth have an wedge shaped leading edge and waves originating from it.

At the higher side of the range of Reynolds number investigated, the originally formed stripe, seeds new stripes into the laminar flow. Two mechanisms are observed for this process: first, *splitting* events are observed for $Re_m = 1450$. In this case the front and the rear part of the stripe disconnect and subsequently grow independently as two parallel stripes. Secondly, stripes are also found to *branch* into the a V-shape for Reynolds numbers as low as 1100.

There is a preferred *natural angle* for turbulent stripes. Stripes produced at a different initial angles either decay rapidly or slowly adjust to a small range around the natural angle. The stripe's natural angle shows a clear trend and decreases from 45° to 25° in the range $900 < Re_m < 1500$.

It has thus been established that turbulent stripes are the relevant localized structures in the transitional range. At low Re_m they start decaying from the trailing edge. Conversely, they grow from their leading edge and, in addition, spread by splitting and branching. In general, the competition between these process decides whether turbulence ultimately decays or grows. The overall growth rates can be estimated as a function of Reynolds number by ensemble average of the turbulent fraction. Hence the critical Re for sustained turbulence is found in the range $950 < Re_m < 1000$. Notably, this is far below all previous estimates.

4.2 Outlook

This study demonstrated the importance of a suitable initial perturbation for studying localised turbulence at low Reynolds numbers. The perturbation must ensure the formation of a well-established stripe as described earlier. Hence *quench* experiments, where a stripe is generated in a high Reynolds number flow and then is introduced into an area of low-Reynolds number, would complement the present result.

This study suggested the existence of the critical point in an entirely different range of Reynolds numbers than reported in previous work. In order to narrow down the critical point a channel of even larger aspect ratio and longer observation time would be required to distinguish smaller changes in turbulent fraction.

Future work on the behaviour of localised turbulence could focus on a higher range of Reynolds numbers to study the transition from intermittent to fully turbulent flow. It would be the obvious next step to extend this study to the interaction between stripes and the formation of patterns, as well as the influence of these interactions on the critical Reynolds number. Consequently, the analogy of a percolation-like phase transition at the critical point could be explored. However, due to advection this would be particularly challenging in experiments since much longer observation times are needed.

Bibliography

- [1] S. Bottin, O. Dauchot, and F. Daviaud. Intermittency in a locally forced plane Couette flow. *Phys. Rev. Lett.*, 79:4377–4380, 1997.
- [2] P. Manneville and F. Locher. A model for transitional plane Couette flow. *Comptes Rendus de l'Académie des Sciences - Séries IIB*, 328:159–164, 2000.
- [3] Y. Duguet A. Monokrousos, L. Brandt, and D.S. Henningson. Minimal transition threshold in plane Couette flow. *Phys. Fluids*, 25:084103, 2013.
- [4] P. Manneville. Spatiotemporal perspective on the decay of turbulence in wall-bounded flows. *Phys. Rev. E*, 79:025301, 2009.
- [5] Y. Pomeau. *Physica D*, 23, 1986.
- [6] J. Philip and P. Manneville. From temporal to spatiotemporal dynamics in transitional plane Couette flow. *Phys. Rev. E*, 83:036308, 2011.
- [7] T.M. Schneider, D. Marinc, and B. Eckhardt. Localised edge states nucleate turbulence in extended plane Couette flow. *J. Fluid Mech.*, 646: 441–451, 2010.
- [8] Y. Duguet, P. Schlatter, and D.S. Henningson. Formation of turbulent patterns near the onset of transition in plane Couette flow. *J. Fluid Mech.*, 650:119–129, 2010.
- [9] P. Manneville and J. Rolland. Transition to turbulence in globally subcritical systems. In *19ème Congrès Français de Mécanique, Marseilles*, 2009.
- [10] O. Reynolds. An experimental investigation of the circumstances which determine whether the motion of water shall be direct or sinuous, and

- of resistance in parallel channels. *Phil. Trans. R. Soc. Lond. Ser. A*, 174: 935–982, 1883.
- [11] P. Manneville. Turbulent-laminar patterns in plane Poiseuille flow. *Eur. J. Mech. B. ArXiv:1403.6374v1*, 2014.
- [12] P.G. Drazin and W.H. Reid. *An Introduction to Hydrodynamic Stability Theory*. Cambridge University Press, Cambridge, UK, 1980.
- [13] R.R. Kerswell. Recent progress in understanding the transition to turbulence in a pipe. *Nonlinearity*, 18:17–44, 2005.
- [14] W. Pfenninger. Transition in the inlet length of tubes at high Reynolds numbers. *Boundary Layer and Flow Control*, pages 970–980, 1961.
- [15] I.J. Wygnanski and F.H. Champagne. On transition in a pipe. Part 1. The origin of puffs and slugs and the flow in a turbulent slug. *J. Fluid Mech*, 59:281–335, 1973.
- [16] I.J. Wygnanski, M. Sokolov, and D. Friedman. On transition in a pipe. Part 2. The equilibrium puff. *J. Fluid Mech*, 69:283–304, 1975.
- [17] B. Hof, J. Westerweel, T.M. Schneider, and B. Eckhardt. Finite lifetime of turbulence in shear flows. *Nature*, 443:59–62, 7 September 2006.
- [18] K. Avila, D. Moxey, A. de Lozar, M. Avila, D. Barkley, and B. Hof. The onset of turbulence in pipe flow. *Science*, 333:192–196, 8 July 2011.
- [19] H.W. Emmons. The laminar-turbulent transition in a boundary layer - Part I. *J. Aero. Sci.*, 18:490–498, 1951.
- [20] D. Coles. Transition in circular Couette flow. *J. Fluid Mech.*, 21:385–425, 1965.
- [21] A. Lundbladh and A.V. Johansson. Direct simulations of turbulent spots in plane Couette flow. *J. Fluid Mech.*, 229:499–516, 1991.
- [22] N. Tillmark and P.H. Alfredsson. Experiments on transition in plane Couette flow. *J. Fluid Mech.*, 235:89–102, 1992.

- [23] D.R. Carlson, S.E. Widnall, and M.F. Peeters. A flow-visualisation study of transition in plane Poiseuille flow. *J. Fluid Mech.*, 121:487–505, 1982.
- [24] H. Schlichting. *Boundary Layer Theory, 6th edition*. McGraw-Hill, 1968.
- [25] S.A. Orszag. Accurate solution of the Orr-Sommerfeld stability equation. *J. Fluid Mech.*, 50:689–703, 1971.
- [26] T. Tsukahara, K. Iwamoto, H. Kawamura, and T. Takeda. DNS of heat transfer in a transitional channel flow accompanied by a turbulent puff-like structure. In *Proc. of the 5th Int. Symp. on Turbulence, Heat and Mass Transfer, Dubrovnik, 2006*.
- [27] F. Alvayoon, D.S. Henningson, and P.H. Alfredsson. Turbulent spots in plane Poiseuille flow-flow visualisation. *Phys. Fluids A*, 29:1328–1331, 1986.
- [28] B.G.B. Klingmann and P.H. Alfredsson. Turbulent spots in plane Poiseuille flow - measurements of the velocity field. *Phys. Fluids A*, 2: 2183–2195, 1990.
- [29] T. Tsukahara, Y. Seki, H. Kawamura, and D. Tochio. DNS of turbulent channel flow at very low Reynolds numbers. In *Proc. of the 4th Int. Symp. on Turbulence and Shear Flow Phenomena, Williamsburg, 2005*.
- [30] S. Hashimoto, A. Hasobe, T. Tsukahara, Y. Kawaguchi, and H. Kawamura. An experimental study on turbulent-stripe structure in transitional channel flow. In *Proc. of the 6th Int. Symp. on Turbulence, Heat and Mass Transfer, Rome, 2009*.
- [31] H. Aida, T. Tsukahara, and Y. Kawaguchi. Development of a turbulent spot in a stripe pattern in plane Poiseuille flow. In *Proc. of the 7th Int. Symp. on Turbulence and Shear Flow Phenomena, 2011*.
- [32] D. Seki and M. Matsubara. Experimental investigation of relaminarizing and transitional channel flows. *Physics of Fluids*, 24:124102, 2012.

- [33] L.S. Tuckerman, T. Kreilos, H. Schrobsdorff, T.M. Schneider, and J.F. Gibson. Turbulent-laminar patterns in plane Poiseuille flow. *ArXiv:1404.1502v1*, 2014.
- [34] F. Waleffe. Homotropy of exact coherent structures in plane shear flow. *Phys. Fluids*, 15:1517, 2003.
- [35] D. Barkley and L.S. Tuckerman. Computational study of turbulent laminar patterns in Couette flow. *Phys. Rev. Lett.*, 94:014502, 2005.
- [36] L.S. Tuckerman and D. Barkley. Patterns and dynamics in transitional plane Couette flow. *Phys. Fluids*, 23:041301, 2011.
- [37] Y. Duguet and P. Schlatter. Stochastic and deterministic motion of a laminar-turbulent front in a spanwisely extended Couette flow. *Physical Review E*, 84:034502, 2011.
- [38] Y. Duguet and P. Schlatter. Oblique laminar-turbulent interfaces in plane shear flows. *Phys. Rev. Lett.*, 110:034502, 2013.
- [39] J.C. Russ. *The Image Processing Handbook, 3rd edition*. Taylor and Francis, 1998.
- [40] S. Bottin and H. Chaté. Statistical analysis of the transition to turbulence in plane Couette flow. *European Physical Journal B*, 6:143–155, 1998.
- [41] D.S. Henningson and P.H. Alfredsson. The wave structure of turbulent spots in plane Poiseuille flow. *J. Fluid Mech.*, 178:405–421, 1987.

Curriculum Vitae

Personal Data

Name	Michael Philip SITTE
Date of birth	18 December 1989
Place of birth	Vienna
Nationality	Austrian
Address	Freyung 6/4, 1010 Vienna, Austria
Email	michael-philip.sitte@centraliens.net

Education

10/2013-present	Vienna University of Technology M.Sc. in Mechanical Engineering
10/2012-10/2013	University of Cambridge M.Phil. in Energy Technologies Dissertation: "Application of an ignition model to a premixed single burner and an annular combustor" Supervisor: Prof. Epaminondas Mastorakos
09/2010-06/2012	Ecole Centrale Paris Diplôme d'Ingénieur
10/2008-07/2010	Vienna University of Technology B.Sc. in Mechanical Engineering
09/2000-06/2008	Secondary School Gymnasium Rahlgasse, Vienna

Professional Experience

10/2013-02/2014	Teaching Assistant at Inst. for Mechanics , Vienna
07/2012-08/2012	Intern at Schlumberger Ltd. , Ploiesti, Romania
07/2011-08/2011	Intern at Steyr Motors GmbH , Steyr, Austria